nature cell biology

ARTICLES

https://doi.org/10.1038/s41556-018-0127-y

Senescence-associated ribosome biogenesis defects contributes to cell cycle arrest through the Rb pathway

Frédéric Lessard[1], Sebastian Igelmann[1], Christian Trahan[2], Geneviève Huot[1], Emmanuelle Saint-Germain[1], Lian Mignacca[1], Neylen Del Toro[1], Stéphane Lopes-Paciencia[1], Benjamin Le Calvé[5], Marinieve Montero[1], Xavier Deschênes-Simard[4], Marina Bury[6], Olga Moiseeva[7], Marie-Camille Rowell[1], Cornelia E. Zorca[1], Daniel Zenklusen[1], Léa Brakier-Gingras[1], Véronique Bourdeau[1], Marlene Oeffinger[1,2,3] and Gerardo Ferbeyre[1]*

Cellular senescence is a tumour suppressor programme characterized by a stable cell cycle arrest. Here we report that cellular senescence triggered by a variety of stimuli leads to diminished ribosome biogenesis and the accumulation of both rRNA precursors and ribosomal proteins. These defects were associated with reduced expression of several ribosome biogenesis factors, the knockdown of which was also sufficient to induce senescence. Genetic analysis revealed that Rb but not p53 was required for the senescence response to altered ribosome biogenesis. Mechanistically, the ribosomal protein S14 (RPS14 or uS11) accumulates in the soluble non-ribosomal fraction of senescent cells, where it binds and inhibits CDK4 (cyclin-dependent kinase 4). Overexpression of RPS14 is sufficient to inhibit Rb phosphorylation, inducing cell cycle arrest and senescence. Here we describe a mechanism for maintaining the senescent cell cycle arrest that may be relevant for cancer therapy, as well as biomarkers to identify senescent cells.

Cellular senescence opposes neoplastic transformation by preventing the proliferation of cells that have experienced oncogenic stimuli[1]. Senescence is efficient as a tumour suppressor mechanism as long as it prevents cell cycle progression. Some benign lesions contain senescent cells that remain out of the cell cycle[2,3]. Senescent cells also stimulate their own clearance by the immune system, thereby strengthening the defenses against tumourigenesis[4,5]. However, the process is not infallible and lesions containing senescent cells can progress into malignant cancers[6,7]. To escape from senescence, cells need to increase protein biosynthesis and, more importantly, the machinery to do so. Indeed, ribosome biogenesis is upregulated in cancer cells[8,9]. Senescent cells exhibit reduced ribosome biogenesis and this has been explained by a delay in ribosomal RNA (rRNA) processing eventually leading to the accumulation of the ribosomal proteins L5 (uL18) and L11 (uL5), which form a complex with the 5S rRNA and disable the E3 ligase MDM2 (or HDM2), thus activating p53[10]. Conversely, drugs that reduce ribosome biogenesis can trigger senescence and are considered very promising anticancer therapeutics[11–13].

Cellular senescence can be induced in cells in the absence of p53[14] through a pathway that involves several members of the cyclin-dependent kinase inhibitor (CKI) family, such as p16INK4a (p16) and p15INK4b (or CDKN2B), and the retinoblastoma (Rb1 or Rb) tumour suppressor[15,16]. Rb controls cell cycle progression by repressing E2F activity, and in senescent cells, by promoting the formation of heterochromatin at E2F target promoters[3,17]. In proliferating cells or cells that escape from senescence, Rb is inhibited by cyclin-dependent kinases such as CDK2, CDK4 and CDK6[18]. Genetic inactivation of CDK4 leads to p53-independent senescence[18] and CDK4 inhibitors can reactivate a latent senescence programme in cancer cells[19,20]. Here, we show a mechanism that targets the CDK4/6 kinases in senescent cells. We demonstrate that oncogenic signals interfere with rRNA biogenesis via the degradation of multiple ribosome biogenesis factors, leading to a p53-independent but Rb-dependent senescence response. Senescent cells accumulated both rRNA precursors and ribosomal proteins in the nucleus and nucleolus. Moreover, we found that the ribosomal protein S14 (uS11) binds and inactivates the cyclin-dependent kinase CDK4, thereby acting as a CKI and linking ribosome biogenesis to cell cycle control. Since p53 is inactivated in most human cancers, this work provides a rationale to target ribosome biogenesis and restore senescence in human tumours in a p53-independent manner.

Results

Deficient ribosome biogenesis and accumulation of rRNA precursors in senescent cells. Non-dividing cells as well as senescent cells have a limited demand for ribosomes and hence ribosome biogenesis. Paradoxically, induction of senescence by oncogenic *Ras* or by telomere shortening (replicative senescence) in normal human fibroblasts induces nucleolar clustering into a single prominent nucleolus (Fig. 1a), reminiscent of big and abundant nucleoli of aggressive cancer cells[9]. To determine the relationship between decreased ribosome biogenesis and the senescence programme, we first used the model of oncogene-induced senescence (OIS). Shortly after the introduction

[1]Department of Biochemistry and Molecular Medicine, Université de Montréal, Montreal, Quebec, Canada. [2]Institut de Recherches Cliniques de Montréal, Montreal, Quebec, Canada. [3]Faculty of Medicine, Division of Experimental Medicine, McGill University, Montreal, Quebec, Canada. [4]Faculty of Medicine, Department of Medicine, McGill University, Montreal, Quebec, Canada. [5]URBC-NARILIS, University of Namur, Namur, Belgium. [6]Lady Davis Institute for Medical Research, McGill University, Montreal, Quebec, Canada. [7]Generium 601125 Vladimirskaya obl, Petushinsky, Russia. *e-mail: g.ferbeyre@umontreal.ca

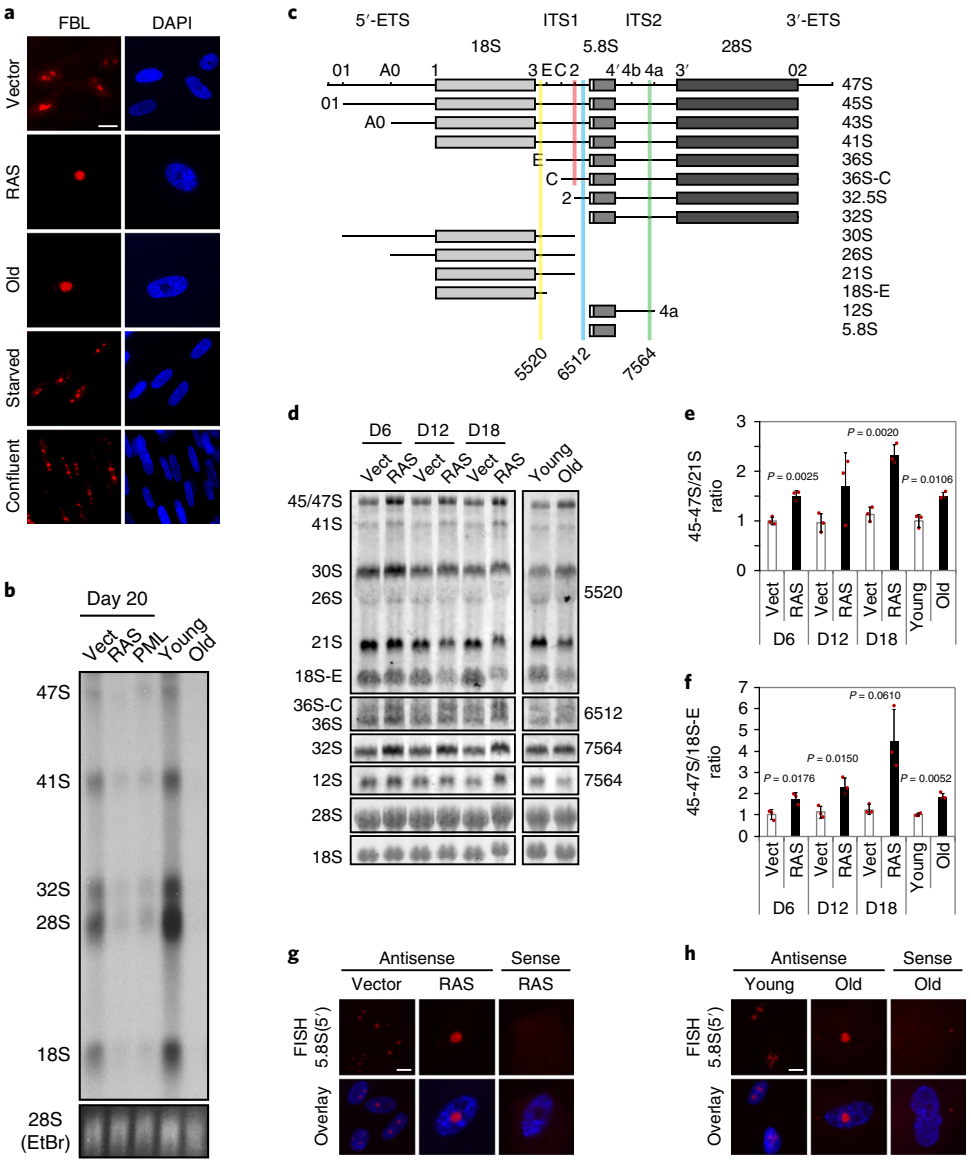

Fig. 1 | Senescence involves diminished ribosome biogenesis. a, Indirect immunofluorescence (IF) with a specific anti-fibrillarin (FBL) antibody showing the nucleolus. The nucleus was counterstained with DAPI. Images represent IMR90 cells expressing an empty control vector or H-RASV12 (RAS) at day 12 post-infection, IMR90 cells at replicative senescence (old) (passage 40), serum starved for 6 days or confluent arrested for 4 days (1 out of 3 independent experiments with similar results). Scale bar, 20 µm. **b**, Autoradiography for de novo rRNA synthesis after a three-hour pulse labelling with [^{3}H]-uridine. Total RNA was extracted after the pulse from IMR90 cells at day 20 post-infection with H-RASV12 (RAS), PML-IV (PML) or an empty control vector (Vect), or young (passage 24) and old (passage 38) IMR90 cells and compared to total 28S rRNA detected with ethidium bromide (EtBr) under UV light (1 out of 3 independent experiments with similar results). **c**, Schematic representation of the human 47S rRNA and different rRNA processing intermediates. The regions used for northern probes (yellow, position 5520; blue, position 6512; green, position 7564) and FISH (red) are indicated. **d**, Northern blots with total RNA extracted from IMR90 cells at day 6, day 12 and day 18 post-infection with H-RASV12 (RAS) or an empty control vector (Vect), or young (passage 24) and old (passage 40) IMR90 cells (1 out of 3 independent experiments with similar results). Precursor rRNAs detected with the probes described in **c** are indicated (right). **e**,**f**, Ratios of 45–47S/21S (**e**) and 45–47S/18S-E (**f**) rRNA levels quantified from experiments as in **d**. All signals were normalized to total 28S rRNA detected with methylene blue staining. Error bars are mean ± s.d., $n = 3$ independent experiments. *P* value as indicated, two-sided Student's *t*-test. **g**,**h**, Fluorescence in situ hybridization (FISH) with an antisense or sense probe overlapping the 5.8S (5′) rRNA processing site 2 as shown in **c**. The nucleus was counterstained with DAPI. Images represent MR90 cells expressing H-RASV12 (RAS) or an empty control vector at day 20 post-infection (**g**) or young (passage 25) and old (passage 43) IMR90 cells (**h**) (1 out of 2 independent experiments with similar results). Scale bars (**g**,**h**), 10 µm. See also Supplementary Figs. 1 and 2.

of oncogenic *Ras*, there is an increase in both rRNA synthesis and cell proliferation (days 2–6, Supplementary Fig. 1a). However, when cells became senescent (days 8–20 after Ras expression, PML (promyelocytic leukaemia) expression or telomere shortening), rRNA synthesis was dramatically reduced as measured using a three-hour pulse of ^{3}H-uridine (Fig. 1b and Supplementary Fig. 1a–d). We conclude that the synthesis of rRNA is largely reduced in senescent cells irrespective of the stress that triggered the process.

Next, we used probes complementary to the internal transcribed spacers ITS1 and ITS2 (Fig. 1c) to characterize pre-rRNA processing intermediates in senescent cells. We loaded the gels normalized against the amount of mature 28S rRNA as was done for pulse

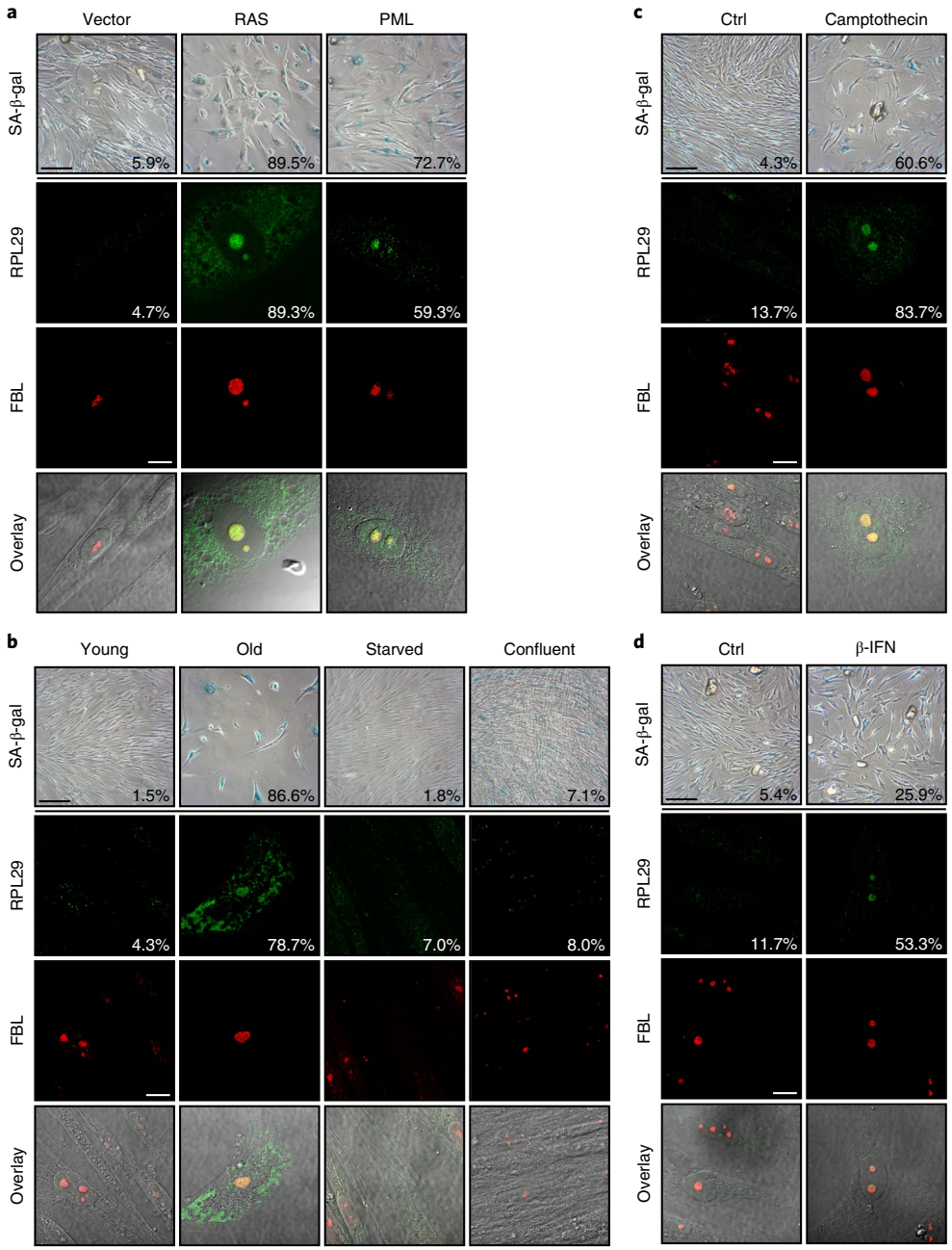

Fig. 2 | Accumulation of RPL29 as a senescence biomarker. SA-β-gal and IF (indirect immunofluorescence) for RPL29 and fibrillarin (FBL) nucleolar colocalization in IMR90 cells with the indicated treatment of cells. SA-β-gal data were quantified from >5 independent cell counts up to a total of at least 150 cells and are presented as the mean percentage of positive cells. IF data were quantified from 100 cell counts in triplicates and are presented as the mean percentage of cells with nucleolar localization of RPL29. Scale bars: SA-β-gal, 200 µm; IF, 20 µm. **a**, Comparison of IMR90 cells expressing H-RASV12 (RAS), PML-IV (PML) or an empty control vector and fixed at day 12 post-infection (1 out of 3 independent experiments with similar results). **b**, Comparison of young (passage 23), old (passage 40), serum starved for 6 days and confluent arrested for 4 days IMR90 cells (1 out of 3 independent experiments with similar results). **c**, Comparison of IMR90 cells treated for 3 days with DMSO (ctrl) or camptothecin in DMSO (final concentration in medium of 35 nM) (1 out of 3 independent experiments with similar results). **d**, Comparison of IMR90 cells treated every 2–3 days with vehicle (ctrl) or β-IFN (final concentration in the medium of 1,000 U ml^{-1}) for 14 days (1 out of 2 independent experiments with similar results).

labelling in Fig. 1b. While we observed a general decrease in rRNA synthesis in *ras*-senescent cells and old (replicative senescent) cells by pulse labelling (Fig. 1b and Supplementary Fig. 1a), we did not detect a similar decrease in rRNA precursors at steady state by northern blotting. The primary rRNA precursor, 47S, accumulated in senescent cells, while the levels of the small subunit intermediates 21S and 18S-E decreased (Fig. 1d). Consequently, senescent cells had increased 47S/21S (Fig. 1e) and 47S/18S-E (Fig. 1f) ratios. This finding is striking given the observed decrease in rRNA synthesis as shown by pulse labelling (Fig. 1b), and is consistent with previous work showing that disabling the small nucleolar RNAs U3 and U8 leads to the accumulation of the 47S rRNA precursor, G1/S cell cycle arrest and nucleolar fusion, which are characteristics of cellular senescence[21]. Additionally, we assessed the accumulation of rRNA precursors in senescent cells using single-cell analysis and RNA-FISH with a probe that detects non-processed rRNA intermediates

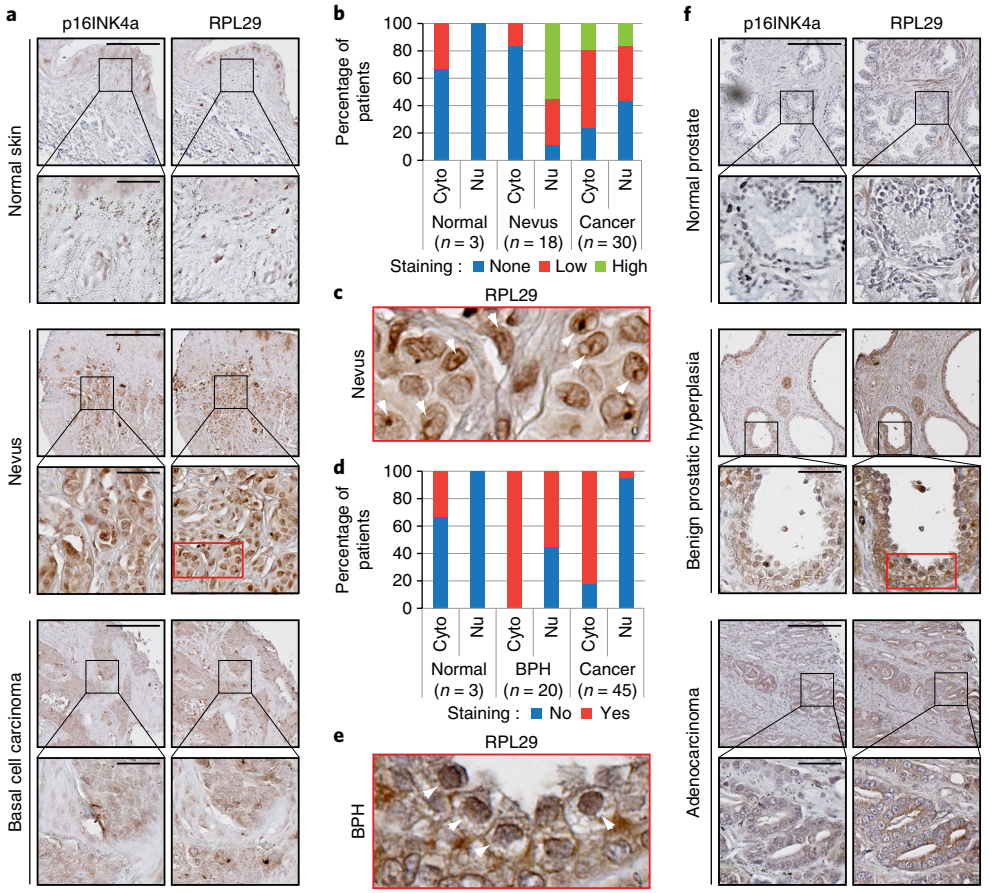

Fig. 3 | Nuclear RPL29, a biomarker of decreased ribosome biogenesis and senescent cells in vivo. a, p16INK4a and RPL29 immunostaining in samples from patients with nevus (middle), normal skin controls (top), or basal cell carcinoma (bottom). Images represent data from 18, 3 and 30 samples, respectively. **b**, Percentage of patient samples immunostained as in **a** showing no RPL29 staining, or with either a cytoplasmic (Cyto) or a nuclear (Nu) RPL29 staining using two different degrees of intensity (low and high). **c**, Enlargement of the red rectangle from nevus (**a**) showing nucleolar staining for RPL29. **d**–**f**, Percentages of patient samples (in **f**) showing no staining, or with either a cytoplasmic (Cyto) or nuclear (Nu) RPL29 staining (**d**). Enlargement of the red rectangle in BPH (benign prostatic hyperplasia) from **f** showing nuclear staining for RPL29 (**e**). p16INK4a and RPL29 immunostaining (**f**) in samples from patients with BPH (middle), normal prostatic controls (top) or prostate adenocarcinoma (bottom). Images represent data from 20, 3 and 45 samples, respectively. Scale bars (**a**,**f**): 250 μm (low magnification) and 50 μm (high magnification).

(Fig. 1c). We found a prominent accumulation of these precursors in the nucleolus of *Ras*-senescent cells, old cells and PML-senescent cells, but not in cells arrested by confluence or serum starvation (Fig. 1g,h and Supplementary Fig. 2). We thus conclude that senescence involves a reduction in both rRNA synthesis and processing.

Nuclear accumulation of ribosomal protein RPL29 is a new biomarker for cellular senescence. It has been reported that some ribosomal proteins (ribosomal protein L29; also known as RPL29 or eL29) accumulate in nucleoli following defects in ribosome biogenesis[22]. Consistently, we found an accumulation of RPL29 in the nucleoli of *Ras*-senescent cells, PML-senescent cells and old cells (Fig. 2a,b), but not in cells arrested by serum starvation or confluence (Fig. 2b). A prominent nucleolus that accumulates RPL29 was also characteristic of the senescence response to camptothecin (therapy-induced senescence) (Fig. 2c) and β-interferon (Fig. 2d).

The consistent accumulation of markers of altered ribosome biogenesis in senescent cells suggested that they could be used as senescence biomarkers in vivo. Towards this goal, we first studied naevi, which are senescent benign lesions[2]. In agreement with our observations from cells in culture, p16INK4a-positive naevi also accumulated RPL29 in their cell nucleus, while little staining was observed in the cell nucleus of normal skin or in basal cell carcinoma lesions, where most of the staining was cytoplasmic (Fig. 3a,b). With magnification, prominent nucleoli positive for RPL29 were observed in naevi cells (Fig. 3c). Similarly, p16INK4a-positive benign prostatic hyperplasia lesions accumulated RPL29 in the cell nucleus, while this biomarker was absent in nuclei of normal prostate epithelial cells or prostate adenocarcinoma cells (Fig. 3d–f).

Cellular senescence involves reduced levels of ribosome biogenesis factors. To investigate the mechanism leading to decreased ribosome biogenesis and ribosomal protein accumulation in senescent cells, we studied the levels of several ribosome biogenesis factors previously found as candidate targets for proteasome dependent senescence-associated protein degradation (SAPD) in *Ras*-induced senescence (Supplementary Fig. 3a)[1,23]. We found that the more unstable ribosome biogenesis factors RSL1D1 (ribosomal L1 domain containing 1)[24], nucleostemin (NS or GNL3)[24,25], DDX21 (DExD-Box helicase 21)[25] and EBP2 (EBNA1 binding protein 2; also known as EBNA1BP2)[25] were downregulated at the protein level in *Ras*-senescent, PML-senescent and old cells (Fig. 4a). However, the mRNAs encoding these proteins were not reduced in senescent cells (Supplementary Fig. 3b–d). RSL1D1 was previously linked to senescence[23,26] and we found many nucleolar proteins interacting with RSL1D1 (Fig. 4b and Supplementary Table 1) including NS, DDX21 and EBP2 (Fig. 4c).

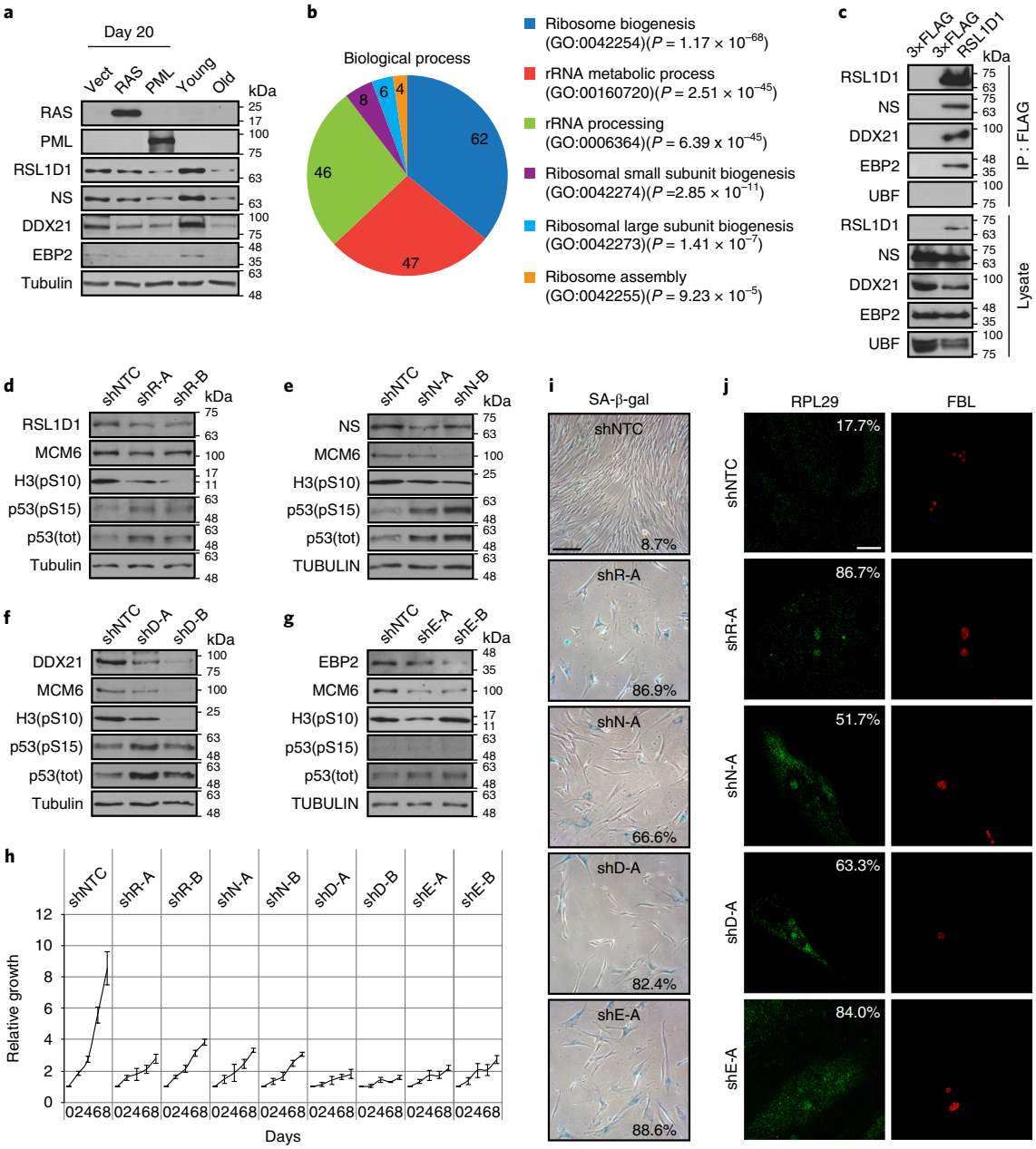

Fig. 4 | Reduction of ribosome biogenesis factors RSL1D1, nucleostemin, EBP2 or DDX21 triggers senescence. a, Immunoblots for the indicated proteins in IMR90 cells at day 20 post-infection with H-RASV12 (RAS), PML-IV (PML) or an empty control vector (Vect) or young (passage 24) and old (passage 38) IMR90 cells. NS, nucleostemin. Tubulin was used as a loading control. **b**, Gene ontology (GO) terms found after FatiGO single-enrichment analysis with the Babelomics 4.3 platform performed on the proteins that were identified by liquid chromatography-tandem mass spectrometry (LC-MS/MS) after immunoprecipitation of 3× FLAG or 3× FLAG-RSL1D1 transiently transfected in HEK-293 cells. **c**, Interactions between RSL1D1 and several ribosome biogenesis factors. HEK-293 cells were transiently transfected with 3× FLAG or 3× FLAG-RSL1D1 vectors and immunoprecipitated with an anti-FLAG antibody. Lysates and immunoprecipitates were immunoblotted for the indicated proteins. **d**–**g**, Immunoblots for the indicated proteins in IMR90 cells expressing the indicated shRNA expression vectors at day 14 post-infection. shNTC, non-targeting shRNA; shR-A or shR-B, shRNAs against RSL1D1; shN-A or shN-B, shRNAs against nucleostemin; shD-A or shD-B, shRNAs against DDX21; shE-A or shE-B, shRNAs against EBP2; H3(pS10), histone H3 phosphorylated on serine 10; p53(pS15), p53 phosphorylated on serine 15; p53(tot), total p53; NS, nucleostemin. Tubulin was used as a loading control. **h**, Growth curves started with cells as in **d**–**g**. Data are presented as means normalized to day 0 of each condition and error bars indicate s.e.m., $n = 3$ independent experiments. **i**, SA-β-gal of IMR90 cells expressing the indicated shRNA expression vectors as in **d**–**g** and fixed at day 14 post-infection. Data were quantified from >5 independent cell counts up to a total of at least 150 cells and are presented as the mean percentage of positive cells (1 out of 3 independent experiments with similar results). Scale bar, 200 µm. **j**, RPL29 and FBL nucleolar localization in IMR90 cells expressing the indicated shRNA expression vectors as in **d**–**g** and fixed at day 7 post-infection. Data were quantified from 100 cell counts in triplicates and are presented as the mean percentage of positives cells for nucleolar localization of RPL29 (1 out of 3 independent experiments with similar results). Scale bar, 20 µm. See also Supplementary Fig. 3. Blots in **a**,**c**,**d**,**e**,**f**,**g** are representative of 3 independent experiments with similar results. Unprocessed blots can be found in Supplementary Fig. 9.

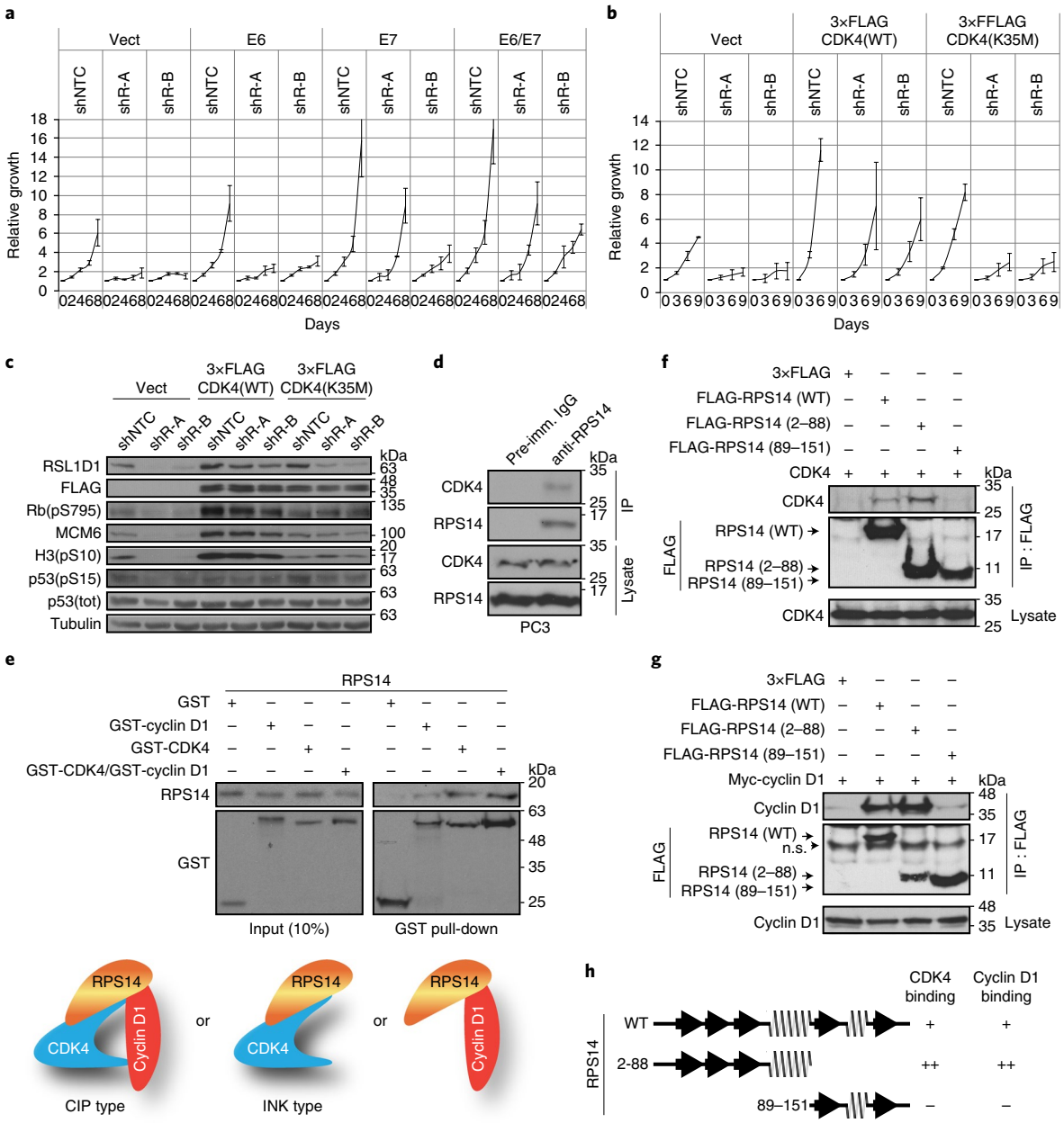

Fig. 5 | E7 and CDK4, but not E6, bypass RSL1D1 knockdown-induced senescence. a, Growth curves of IMR90 cells expressing the indicated shRNA expression vectors in combination with the expression of the viral oncoproteins E6 alone, E7 alone, E6/E7 together or an empty control vector (Vect). Data are presented as mean normalized to day 0 of each condition and error bars indicate s.e.m., $n = 3$ independent experiments. shNTC, non-targeting shRNA; shR-A or shR-B, shRNAs against RSL1D1. **b**, Growth curves of IMR90 cells expressing the indicated shRNA expression vectors as in **a** in combination with the expression of 3× FLAG-CDK4(WT), 3× FLAG-CDK4(K35M) or an empty control vector (Vect). Data are presented as mean normalized to day 0 of each condition and error bars indicate s.e.m., $n = 3$ independent experiments. **c**, Immunoblots for the indicated proteins for cells as in **b** collected 20 days post-infection. Rb(pS795), Rb phosphorylated on serine 795; H3(pS10), histone H3 phosphorylated on serine 10; p53(pS15), p53 phosphorylated on serine 15; p53(tot), total p53. Tubulin was used as a loading control. **d**, Immunoprecipitation with pre-immune serum (Pre-imm. IgG) or with anti-RPS14 antibody in PC3 cells. Lysates and immunoprecipitates were immunoblotted for the indicated proteins. **e**, Top: in vitro GST pulldown of recombinant GST, GST-cyclin D1, GST-CDK4 or GST-CDK4/GST-cyclin D1 and recombinant RPS14-Myc-FLAG using glutathione beads. Lysate and pulldown were immunoblotted for the indicated proteins. Bottom: schematic model showing interactions between RPS14 and cyclin D1, CDK4 or CDK4/cyclin D1. **f**, HEK-293 cells were transfected with vectors expressing CDK4 and 3× FLAG or FLAG-tagged RPS14 wild type (FLAG-RPS14(WT)), FLAG-RPS14(2–88) or FLAG-RPS14(89–151) and immunoprecipitated with an anti-FLAG antibody. Lysates and immunoprecipitates were immunoblotted for indicated proteins. **g**, HEK-293 cells were transfected with a vector expressing Myc-cyclin D1 and vectors expressing 3× FLAG or FLAG-RPS14(WT), FLAG-RPS14(2–88) or FLAG-RPS14(89–151) and immunoprecipitated with an anti-FLAG antibody. Lysates and immunoprecipitates were immunoblotted for indicated proteins (n.s., not specific). **h**, Schematic showing RPS14 regions and their interaction with CDK4 and/or cyclin D1. See also Supplementary Figs. 4, 5 and 6. Blots in **d**–**g** are representative of 3 independent experiments with similar results, whereas **c** is representative of 2 independent experiments with similar results. Unprocessed blots can be found in Supplementary Fig. 9.

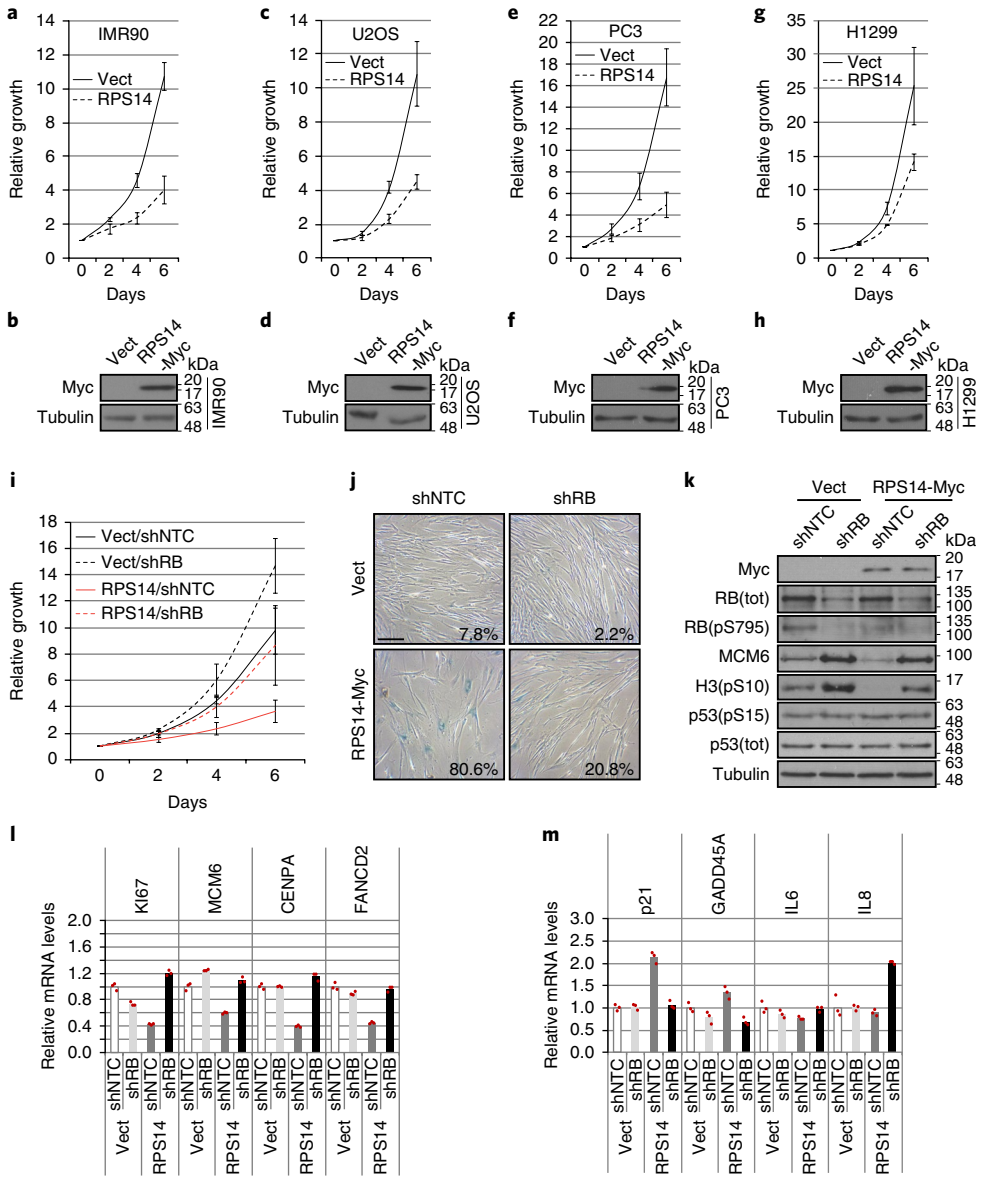

Fig. 6 | RPS14 regulates the retinoblastoma pathway and senescence. a–h, Growth curves (**a**,**c**,**e**,**g**) of IMR90 cells (**a**), U2OS cells (**c**), PC3 cells (**e**) or H1299 cells (**g**) expressing RPS14-Myc or an empty control vector (Vect). Data are presented as mean normalized to day 0 of each condition and error bars indicate s.e.m., $n=3$ independent experiments. Immunoblots for the indicated proteins (**b**,**d**,**f**,**h**) at day 7 post-infection with an empty control vector (Vect) or a vector expressing RPS14-Myc in IMR90 cells (**b**), U2OS cells (**d**), PC3 cells (**f**) or H1299 cells (**h**) (1 out of 3 independent experiments with similar results). Tubulin was used as a loading control. **i**, Growth curves of IMR90 cells expressing a control shRNA (shNTC) or a shRNA against Rb (shRb) in combination with the expression of RPS14-Myc or an empty control vector (Vect). Data are presented as mean normalized to day 0 of each condition and error bars indicate s.e.m., $n=3$ independent experiments. **j**, SA-β-gal of IMR90 cells as in **i** at day 18 post-infection. Data were quantified from >5 independent cell counts up to a total of at least 150 cells and are presented as the mean percentage of positive cells (1 out of 2 independent experiments with similar results). Scale bar, 200 µm. **k**, Immunoblots for the indicated proteins for cells as in **i** at day 16 post-infection (1 out of 2 independent experiments with similar results). Rb(tot), total Rb; Rb(pS795), Rb phosphorylated on serine 795; H3(pS10), histone H3 phosphorylated on serine 10; p53(pS15), p53 phosphorylated on serine 15; p53(tot), total p53. **l**,**m**, q-PCR for the indicated genes performed on reverse-transcribed total RNA extracted from cells as in **i** at day 16 post-infection. Data are normalized over TBP and HMBS and presented as mean relative to vector infected cells (1 out of 2 independent experiments with similar results). See also Supplementary Fig. 6. Unprocessed blots can be found in Supplementary Fig. 9.

Next, we characterized the effects of directly decreasing the ribosome biogenesis factors RSL1D1, NS, DDX21 or EBP2 using shRNAs (Fig. 4d–g and Supplementary Fig. 3e). Depletion of these factors induced a proliferation arrest (Fig. 4h), a decrease in the proliferation markers KI67 and CENPA (Supplementary Fig. 3f–g), and an increase in senescence-associated β-galactosidase staining (SA-β-gal) (Fig. 4i and Supplementary Fig. 3h). Immunoblots of cell extracts from these senescent cells showed signs of activation of both the p53 and the Rb pathways as assessed by measuring both total and Ser15-phosphorylated p53 levels (Fig. 4d–g). Additionally, we observed a reduction in E2F target genes such as MCM6 and CENPA (Fig. 4d–g and Supplementary Fig. 3g), and an accumulation of p21 (Supplementary Fig. 3i). In contrast, p16INK4a was not consistently increased by shRNAs that depleted ribosome biogenesis factors (Supplementary Fig. 3j). Moreover, knockdown of RSL1D1, NS, DDX21 or EBP2 led to accumulation of RPL29 in the

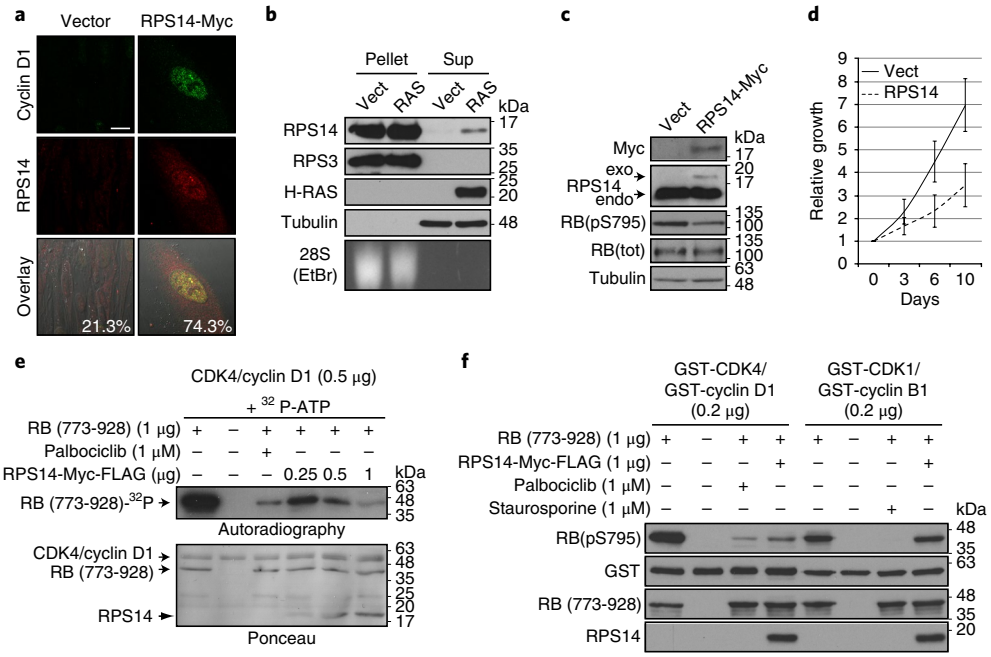

Fig. 7 | RPS14 regulates senescence by inhibiting CDK4. a, RPS14 and cyclin D1 nuclear colocalization in IMR90 cells expressing RPS14-MYC or an empty control vector and fixed at day 14 post-infection, as revealed by indirect immunofluorescence with specific anti-RPS14 and anti-cyclin D1 antibodies followed by confocal microscopy. Data were quantified from 100 cell counts in triplicate and are presented as the mean percentage of positive cells for colocalization (1 out of 3 independent experiments with similar results). Scale bar, 20 µm. **b**, Immunoblots for the indicated proteins and 28S rRNA detected with ethidium bromide (EtBr) following ribosome purification by sedimentation of extracts from IMR90 cells at day 7 post-infection with H-RASV12 (RAS) or an empty control vector (Vect). Pellet, ribosomes; Sup, supernatant. **c**, Immunoblots for the indicated proteins in MUTZ-8 cells expressing RPS14-Myc or an empty control vector (Vect) at day 8 post-infection. Rb(tot), total Rb; Rb(pS795), Rb phosphorylated on serine 795; exo, size for exogenous RPS14; endo, size for endogenous RPS14. **d**, Growth curves for cells as in **c**. Data are presented as mean normalized to day 0 of each condition and error bars indicate s.e.m., $n = 3$ independent experiments. **e**, In vitro kinase assay containing ^{32}P-ATP, GST-CDK4/GST-cyclin D1, with or without GST-Rb (773-928), palbociclib and RPS14-Myc-FLAG. In the assay conditions, the RPS14 IC50 ± s.d. = 0.421 ± 0.088 µM. **f**, Immunoblots for the indicated proteins after an in vitro kinase assay containing ATP, GST-CDK4/GST-cyclin D1 or GST-CDK1/GST-cyclin B1, with or without GST-Rb (773-928), palbociclib, staurosporine and RPS14-Myc-FLAG. Rb(pS795), Rb phosphorylated on serine 795. See also Supplementary Figs. 7 and 8. Blots in **b**,**c**,**e**,**f** are representative of 3 independent experiments with similar results. Unprocessed blots can be found in Supplementary Fig. 9.

nucleolus (Fig. 4j and Supplementary Fig. 3k). We thus conclude that decreasing ribosome biogenesis factors is sufficient to trigger cellular senescence.

Ribosome biogenesis defects engage the retinoblastoma tumour suppressor pathway. To investigate the signalling pathways linking reduced ribosome biogenesis to cellular senescence, we prepared IMR90 cells expressing a combination of papillomavirus oncoproteins E6 and E7, E6 alone or E7 alone. The E6 oncoprotein is known to block p53 functions, whereas E7 deactivates the Rb pathway[27]. In our model, E6 and E7 combined or E7 alone efficiently prevented senescence after knockdown of RSL1D1, while E6 had only a partial effect (Fig. 5a and Supplementary Fig. 4a–e). These results suggest that defects in ribosome biogenesis mainly engage the Rb pathway in human cells. To validate this conclusion, we used mutants of E7 that differ in their ability to block Rb functions[28]. The E7 mutant Δ79–83, which binds and inhibits Rb, rescued cells from senescence after knockdown of RSL1D1, while mutants E7Δ6–10 and E7Δ21–24 that do not bind Rb were not efficient at inhibiting senescence after knockdown of RSL1D1 (Supplementary Fig. 4f–j). Furthermore, the kinases CDK4 and CDK6, which are able to phosphorylate and inactivate Rb[29], were also capable of preventing senescence after knockdown of RSL1D1 (Fig. 5b,c and Supplementary Fig. 5a–h). Expression of intact CDK4, but not of a catalytically inactive mutant (CDK4(K35M)), efficiently bypassed senescence, preventing the downregulation of Ki67 expression, as well as rescuing Rb phosphorylation and the expression of E2F targets such as CENPA and MCM6 after knockdown of RSL1D1 (Fig. 5b,c and Supplementary Fig. 5i–l). CDK4 expression also increased the levels of the mitotic marker H3-pS10 and reduced the levels of the CKI p21 (Fig. 5c and Supplementary Fig. 5m). Although expression of CDK4/6 kinases inhibited the senescence response to RSL1D1 depletion, shRNAs against p16INK4a or p21 did not have a similar effect (Supplementary Fig. 6a–e), suggesting that additional mechanisms control senescence in these cells at the level of CDK4.

RPS14 connects ribosome biogenesis defects to the retinoblastoma pathway. Altered ribosome biogenesis has been linked to p53 activation, and in mouse cells to p53-dependent senescence[30,31]. Defective ribosome biogenesis allows some ribosomal proteins to accumulate in the nucleoplasm and activate p53 by inhibiting MDM2[30,31]. This mechanism explains p53 activation in cells where ribosome biogenesis factors are depleted and is likely to contribute to p53 activation during OIS. However, our results show that ribosome biogenesis defects in human cells can regulate senescence in a p53-independent but Rb-dependent manner. We reasoned that some ribosomal proteins might activate the Rb pathway perhaps acting as CKIs similarly to p21 or p16INK4a. Since we found that the catalytic activity of CDK4 was required to prevent senescence after RSL1D1 depletion (Fig. 5b,c and Supplementary Fig. 5i–m), we used a catalytically inactive CDK4(K35M) as a bait to examine whether any ribosomal protein can bind CDK4 in senescent cells. The rationale for using an inactive CDK4 allele is driven by the fact that active CDK4 inhibits senescence and induces

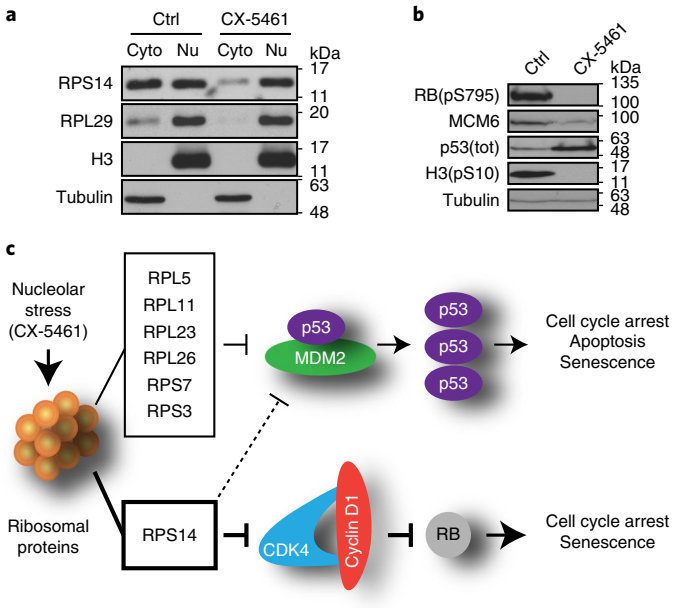

Fig. 8 | Tumour suppression by the RPS14-mediated checkpoint. **a**, Immunoblots for the indicated proteins after cellular fractionation of IMR90 cells treated with dimethylformamide (ctrl) or CX-5461 in dimethylformamide (final concentration in medium of 2 μM) for 24 hours. Cyto, cytoplasm; Nu, nuclear extracts. **b**, Immunoblots for the indicated proteins on total cellular extracts of IMR90 cells treated as in **a**. Rb(pS795), Rb phosphorylated on serine 795; p53(tot), total p53; H3(pS10), histone H3 phosphorylated on serine 10. **c**, Model showing how nucleolar stress and ribosome biogenesis defects can lead to activation of p53 and Rb tumour suppressor pathways. Blots in **a**,**b** are representative of 3 independent experiments with similar results. Unprocessed blots can be found in Supplementary Fig. 9.

cell proliferation. Therefore, any ribosomal protein acting as a CDK inhibitor may cease to do so by getting incorporated into ribosomes in growing cells. We immunoprecipitated flag-tagged CDK4(K35M) from cells that were forced into senescence by depletion of RSL1D1 and identified its partners by mass spectrometry. The CDK4 partners CCND1, CCND3, CDKN1A, CDKN1B, CDKN2B and CDKN2C were found in the immunoprecipitates together with the ribosomal protein RPS14 (Supplementary Table 2). We confirmed that endogenous CDK4 and RPS14 interact in PC3 prostate cancer cells and in H1299 (or NCI-H1299) lung cancer cells (Fig. 5d and Supplementary Fig. 6f). GST pulldown assays with purified proteins revealed that RPS14 binds to either CDK4 or cyclin D1 alone or to the complex of CDK4 with cyclin D1 (Fig. 5e). The interaction data suggests that RPS14 can act both like p16INK4a, an inhibitor of the INK family that binds CDK4, and like p21, a CIP family member, which binds to CDK–cyclin complexes (Fig. 5e). We next mapped the region of RPS14 that binds CDK4 and cyclin D1 by co-immunoprecitation in HEK-293 cells. We found that binding to both CDK4 and cyclin D1 maps to the N-terminal globular core domain (residues 2–88) of RPS14 (Fig. 5f–h), excluding the C-terminal extension that engages in multiple contacts with rRNA via salt bridges between the basic residues of the protein and the phosphate groups of the rRNA[32].

Expression of RPS14 in normal human fibroblasts using retroviral gene transfer induced proliferation arrest (Fig. 6a,b) and several senescence biomarkers, including: an accumulation of flat cells positive for SA-β-gal, a reduction in Rb phosphorylation, a decrease in E2F target gene expression, a reduction in the levels of the mitotic marker H3-pS10, and an accumulation of PML bodies (Supplementary Fig. 6g–n). However, DNA damage foci were only moderately induced by RPS14, similar to p16INK4a expression (Supplementary Fig. 6j,l,m). Ser15-phosphorylated p53, total p53 or p21 levels were not found strongly increased in cells that expressed high levels of RPS14 (Supplementary Fig. 6h,i). Moreover, in p53 wild-type U2OS osteosarcoma cells, stable expression of RPS14 reduced cell proliferation (Fig. 6c,d). However, RPS14 expression also reduced cell proliferation in p53-null PC3 (Fig. 6e,f) and H1299 cells (Fig. 6g,h). Taken together, these results suggest that RPS14 has the capacity to trigger p53-independent cellular senescence by inhibiting the CDK4 kinase and preventing Rb phosphorylation. Of note, the senescence phenotype triggered by RPS14 expression is very similar to that of p16INK4a[33].

RPS14 is a CDK4 inhibitor. Since RPS14 was recovered from the CDK4 immunoprecipitate in senescent cells, we hypothesized that it acted as a CDK inhibitor to trigger senescence via the Rb tumour suppressor pathway. Consistent with this model, RPS14-induced growth arrest and senescence was prevented by shRNAs against Rb (Fig. 6i–m). The activation of Rb by RPS14 was assessed by measuring the levels of the E2F target genes MCM6, CENPA and FANCD2 (Fig. 6k,l). RPS14 expression did not lead to p53 accumulation or to its phosphorylation on serine 15 (Fig. 6k), although we did observe moderate induction of the p53 targets p21 and GADD45A (Fig. 6m). Moreover, as in the cases of p16INK4a- and p21-induced senescence[34], expression of RPS14 did not strongly increase the expression of IL6 or IL8 (Fig. 6m and Supplementary Fig. 6i).

Next, we investigated whether RPS14 colocalized with CDK4/cyclin D1 complexes as expected for a CKI. In normal growing cells endogenous RPS14 is mostly cytosolic, likely in association with ribosomes. However, in cells where RPS14 is overexpressed, we found a significant fraction of this protein in the nucleus colocalizing with cyclin D1 (Fig. 7a). More importantly, the endogenous RPS14 signal in the nucleus was stronger in most of the senescent cell nuclei (over 90%), independent of the stimuli triggering senescence, while control cells only displayed a moderate signal (at most in ~30% of the cells) (Supplementary Fig. 7a–d). Hyperresolution images of RPS14 in senescent cells revealed a fine punctate nuclear pattern (Supplementary Fig. 7e–g). In addition, RPS14 was present in the soluble non-ribosomal fraction of *Ras*-senescent cells (Fig. 7b). These results suggest that a non-ribosomal fraction of the highly abundant RPS14 accumulates in the nucleus of senescent cells, where it can bind and interfere with the functions of the CDK4/cyclin D1 complexes.

Depletion of RPS14 using RNAi is toxic to both normal cells and several tumour cells (Supplementary Fig. 8a–h). RPS14 was previously identified as a haploinsufficient tumour suppressor in the myeloproliferative 5q− syndrome[35]. Cells from these patients have high levels of phosphorylated Rb that can be reduced when RPS14 expression is restored using retroviral gene transfer (Fig. 7c). Of note, the level of expression of exogenous RPS14 is similar to that found in the non-ribosomal fraction of *Ras*-senescent cells and considerably less than the endogenous level. Moreover, adding back RPS14 in 5q− syndrome cells reduced their proliferation (Fig. 7d), as expected for a CKI. These results suggest that a defect in the Rb pathway underlies the 5q− syndrome, and that CDK4/6 inhibitors should restore its functionality in patients.

To investigate whether RPS14 can directly inhibit CDK4, we performed an in vitro kinase assay using purified proteins. As expected, CDK4/cyclin D1 phosphorylates the Rb fragment 773–928 (Fig. 7e). RPS14 inhibited the kinase activity of the CDK4/cyclin D1 complex in a concentration-dependent manner, similar to the CDK4 inhibitor palbociclib (Fig. 7e). In contrast, RPS14 did not inhibit CDK1/cyclin B1 complexes (Fig. 7f), indicating that it acts as a specific CDK4/cyclin D1 inhibitor.

The discovery of a pathway linking reduced ribosome biogenesis to senescence in a p53-independent manner is very important for novel anticancer therapies. In agreement with our findings, use of an RNA polymerase I inhibitor, CX-5461, has been shown to trigger senescence and autophagy in tumour cells lacking p53[11], and cell death in tumour cells that preserve p53[12], with limited toxicity to normal cells[11,12]. We found that shortly after treatment of IMR90 cells with CX-5461, the nuclear/cytoplasmic ratio of both RPL29 and RPS14 increased (Fig. 8a), indicating that a sudden decrease in rRNA synthesis alters the localization of these proteins. In parallel with this change in localization, we found both a reduction in Rb phosphorylation and in the level of the E2F target gene MCM6 (Fig. 8b), suggesting that in these conditions RPS14 could activate the Rb pathway and inhibit cell cycle progression as measured by decreased levels of the mitotic marker H3-pS10 (Fig. 8b). In p53 wild-type cells, such as IMR90, CX-5461 also activates p53 (Fig. 8b). However, in p53-mutant tumour cells, this compound was reported to induce a senescence response[11] that can now be explained by the pathway reported above.

Discussion

Senescent cells are defined by their inability to proliferate and at the same time synthesize and secrete a large amount of proteins[36,37]. Hence, the observed reduction in ribosome biogenesis in these cells does not limit protein synthesis. More exactly, reduced ribosome biogenesis contributes to senescence by triggering a checkpoint that prevents cell cycle progression. First, some ribosomal proteins that cannot be incorporated into ribosomes inhibit MDM2 and activate the p53 pathway[30,31,38,39]. Second, RPS14 accumulates in the nucleus and activates Rb by inhibiting the CDK4/cyclin D1 complex (Fig. 8c). Finally, a reduced capacity for ribosome biogenesis would prevent the growth of any senescent cell that manages to disable the mechanisms of cell cycle arrest.

The identification of RPS14 as a CDK4 inhibitor suggests a tumour suppressor role for this ribosomal protein. Since RPS14 is required for protein biosynthesis, tumours would rely on subtle mechanisms to avoid RPS14-dependent tumour suppression. Indeed, analysis of microarray data available in Oncomine shows a reduction in RPS14 expression in several cancers (Supplementary Fig. 8i–m). Conversely, non-neoplastic naevi, which are benign tumours containing senescent cells, accumulate high levels of RPS14 (Supplementary Fig. 8m). In addition, in testicular cancer, where RPS14 is upregulated, CDK4 is also upregulated, and Rb is downregulated, consistent with the role we propose here for RPS14 in the Rb pathway (Supplementary Fig. 8n). It has been reported that RPS14 also binds MDM2 and contributes to p53 activation during ribosomal stress[40]. However, we found that RPS14 blocks cell proliferation in PC3 prostate cancer cells and H1299 lung cancer cells where the p53 gene is either absent or mutated (Fig. 6e–h). In addition, knockdown of Rb in normal human fibroblasts rescued both the cell cycle arrest and senescence induced by overexpression of RPS14 (Fig. 6i–m). Although in our conditions most of the activity of RPS14 passes through the Rb pathway, its MDM2 inhibitory activity could certainly contribute to tumour suppression in other contexts (Fig. 8c).

A pathway linking reduced ribosome biogenesis to senescence in a p53-independent manner is very important for the development of anticancer therapies, since the p53 pathway is often disabled in cancer cells. We anticipate that targeting rRNA processing will lead to a sudden decrease in ribosome biogenesis and to a massive accumulation of ribosomal proteins selectively in tumour cells, which are already engaged in a highly active ribosome biogenesis programme. Our work thus provides a rationale for a potent and selective anticancer therapy.

Methods

Methods, including statements of data availability and any associated accession codes and references, are available at https://doi.org/10.1038/s41556-018-0127-y.

Received: 25 January 2017; Accepted: 21 May 2018;
Published online: 25 June 2018

References

1. Deschenes-Simard, X., Lessard, F., Gaumont-Leclerc, M. F., Bardeesy, N. & Ferbeyre, G. Cellular senescence and protein degradation: breaking down cancer. *Cell Cycle* **13**, 1840–1858 (2014).
2. Michaloglou, C. et al. BRAFE600-associated senescence-like cell cycle arrest of human naevi. *Nature* **436**, 720–724 (2005).
3. Vernier, M. et al. Regulation of E2Fs and senescence by PML nuclear bodies. *Genes Dev.* **25**, 41–50 (2011).
4. Kang, T. W. et al. Senescence surveillance of pre-malignant hepatocytes limits liver cancer development. *Nature* **479**, 547–551 (2011).
5. Xue, W. et al. Senescence and tumour clearance is triggered by p53 restoration in murine liver carcinomas. *Nature* **445**, 656–660 (2007).
6. Chen, Z. et al. Crucial role of p53-dependent cellular senescence in suppression of Pten-deficient tumorigenesis. *Nature* **436**, 725–730 (2005).
7. Guerra, C. et al. Pancreatitis-induced inflammation contributes to pancreatic cancer by inhibiting oncogene-induced senescence. *Cancer Cell* **19**, 728–739 (2011).
8. Stumpf, C. R. & Ruggero, D. The cancerous translation apparatus. *Curr. Opin. Genet. Dev.* **21**, 474–483 (2011).
9. Bhat, M. et al. Targeting the translation machinery in cancer. *Nat. Rev. Drug Discov.* **14**, 261–278 (2015).
10. Nishimura, K. et al. Perturbation of ribosome biogenesis drives cells into senescence through 5S RNP-mediated p53 activation. *Cell Rep.* **10**, 1310–1323 (2015).
11. Drygin, D. et al. Targeting RNA polymerase I with an oral small molecule CX-5461 inhibits ribosomal RNA synthesis and solid tumor growth. *Cancer Res.* **71**, 1418–1430 (2011).
12. Bywater, M. J. et al. Inhibition of RNA polymerase I as a therapeutic strategy to promote cancer-specific activation of p53. *Cancer Cell* **22**, 51–65 (2012).
13. Devlin, J. R. et al. Combination therapy targeting ribosome biogenesis and mRNA translation synergistically extends survival in MYC-driven lymphoma. *Cancer Discov.* **6**, 59–70 (2016).
14. Serrano, M., Lin, A. W., McCurrach, M. E., Beach, D. & Lowe, S. W. Oncogenic ras provokes premature cell senescence associated with accumulation of p53 and p16INK4a. *Cell* **88**, 593–602 (1997).
15. Ohtani, N. et al. Opposing effects of Ets and Id proteins on p16INK4a expression during cellular senescence. *Nature* **409**, 1067–1070 (2001).
16. Takahashi, A. et al. Mitogenic signalling and the p16INK4a-Rb pathway cooperate to enforce irreversible cellular senescence. *Nat. Cell Biol.* **8**, 1291–1297 (2006).
17. Chicas, A. et al. Dissecting the unique role of the retinoblastoma tumor suppressor during cellular senescence. *Cancer Cell* **17**, 376–387 (2010).
18. Zou, X. et al. Cdk4 disruption renders primary mouse cells resistant to oncogenic transformation, leading to Arf/p53-independent senescence. *Genes Dev.* **16**, 2923–2934 (2002).
19. Acevedo, M. et al. A CDK4/6-dependent epigenetic mechanism protects cancer cells from PML-induced senescence. *Cancer Res.* **76**, 3252–3264 (2016).
20. Goel, S. et al. Overcoming therapeutic resistance in HER2-positive breast cancers with CDK4/6 inhibitors. *Cancer Cell* **29**, 255–269 (2016).
21. Langhendries, J. L., Nicolas, E., Doumont, G., Goldman, S. & Lafontaine, D. L. The human box C/D snoRNAs U3 and U8 are required for pre-rRNA processing and tumorigenesis. *Oncotarget* **7**, 59519–59534 (2016).
22. Wild, T. et al. A protein inventory of human ribosome biogenesis reveals an essential function of exportin 5 in 60S subunit export. *PLoS Biol.* **8**, e1000522 (2010).
23. Deschenes-Simard, X. et al. Tumor suppressor activity of the ERK/MAPK pathway by promoting selective protein degradation. *Genes Dev.* **27**, 900–915 (2013).
24. Meng, L., Yasumoto, H. & Tsai, R. Y. Multiple controls regulate nucleostemin partitioning between nucleolus and nucleoplasm. *J. Cell Sci.* **119**, 5124–5136 (2006).
25. Romanova, L. et al. Critical role of nucleostemin in pre-rRNA processing. *J. Biol. Chem.* **284**, 4968–4977 (2009).
26. Ma, L. et al. CSIG inhibits PTEN translation in replicative senescence. *Mol. Cell Biol.* **28**, 6290–6301 (2008).
27. Mallette, F. A., Goumard, S., Gaumont-Leclerc, M. F., Moiseeva, O. & Ferbeyre, G. Human fibroblasts require the Rb family of tumor suppressors, but notp53, for PML-induced senescence. *Oncogene* **23**, 91–99 (2004).
28. Helt, A. M. & Galloway, D. A. Destabilization of the retinoblastoma tumor suppressor by human papillomavirus type 16 E7 is not sufficient to overcome cell cycle arrest in human keratinocytes. *J. Virol.* **75**, 6737–6747 (2001).
29. Malumbres, M. & Barbacid, M. Cell cycle, CDKs and cancer: a changing paradigm. *Nat. Rev. Cancer* **9**, 153–166 (2009).

30. Donati, G., Peddigari, S., Mercer, C. A. & Thomas, G. 5S ribosomal RNA is an essential component of a nascent ribosomal precursor complex that regulates the Hdm2-p53 checkpoint. *Cell Rep.* **4**, 87–98 (2013).
31. Sloan, K. E., Bohnsack, M. T. & Watkins, N. J. The 5S RNP couples p53 homeostasis to ribosome biogenesis and nucleolar stress. *Cell Rep.* **5**, 237–247 (2013).
32. Rabl, J., Leibundgut, M., Ataide, S. F., Haag, A. & Ban, N. Crystal structure of the eukaryotic 40S ribosomal subunit in complex with initiation factor 1. *Science* **331**, 730–736 (2011).
33. Rodier, F. et al. Persistent DNA damage signalling triggers senescence-associated inflammatory cytokine secretion. *Nat. Cell Biol.* **11**, 973–979 (2009).
34. Coppe, J. P. et al. Tumor suppressor and aging biomarkerp16(INK4a) induces cellular senescence without the associated inflammatory secretory phenotype. *J. Biol. Chem.* **286**, 36396–36403 (2011).
35. Ebert, B. L. et al. Identification of RPS14 as a 5q− syndrome gene by RNA interference screen. *Nature* **451**, 335–339 (2008).
36. Dorr, J. R. et al. Synthetic lethal metabolic targeting of cellular senescence in cancer therapy. *Nature* **501**, 421–425 (2013).
37. Coppe, J. P. et al. Senescence-associated secretory phenotypes reveal cell-nonautonomous functions of oncogenic RAS and the p53 tumor suppressor. *PLoS Biol.* **6**, 2853–2868 (2008).
38. Horn, H. F. & Vousden, K. H. Cooperation between the ribosomal proteins L5 and L11 in the p53 pathway. *Oncogene* **27**, 5774–5784 (2008).
39. Marechal, V., Elenbaas, B., Piette, J., Nicolas, J. C. & Levine, A. J. The ribosomal L5 protein is associated with mdm-2 and mdm-2-p53 complexes. *Mol. Cell Biol.* **14**, 7414–7420 (1994).
40. Zhou, X., Hao, Q., Liao, J., Zhang, Q. & Lu, H. Ribosomal protein S14 unties the MDM2-p53 loop upon ribosomal stress. *Oncogene* **32**, 388–396 (2013).

Acknowledgements

We thank D. P. Baker (Biogen Idec), D. A. Galloway (Fred Hutchinson Cancer Center), N. Bardeesy (MGH), S. Lowe (MSK), A. Koff (MSK), T. Moss (U. Laval), I. Topisirovic, P. Chartrand (U. Montréal), V. Blank (McGill University) and B. Weinberg (MIT) for comments and/or reagents. We thank É. Bonneil, F. McManus and the IRIC Proteomics Core Facility for proteomic analysis. We thank J. Hinsinger, M. Birlea and the IRIC Histology Core Facility for immunohistochemistry. F.L. is supported by FRQS (Fonds de Recherche du Québec-Santé) and the CRS (Cancer Research Society). G.F. is supported by FRQS. Work was funded by grants from the CIHR (Canadian Institute of Health and Research: CIHR MOP11151) to G.F., (Canadian Institutes of Health Research: CIHR MOP106628) to M.O. and the CCSRI (Canadian Cancer Society Research Institute: 704223) to G.F.

Author contributions

F.L. performed most of the cell culture experiments, IHC experiments, immunoprecipitation, cellular fractionation, kinase assays, pulldown, western blots, pulse labelling, SA-β-gal, growth curves, data analysis and northern blotting in collaboration. S.I. performed all the immunofluorescences, bioinformatics analysis of data from LC-MS/MS, helped in quantification of SA-β-gal, IHC and FISH. He also confirmed RPS14 senescence and the bypass by shRB. C.T. performed the northern blotting. G.H. made pBABE-3×FLAG-CDK4(WT) and pBABE-3×FLAG-CDK4(K35M), performed many qPCR and performed cell culture experiments leading to Fig. 5a, Fig. 6a,i–m, Supplementary Figs. 4, 6g–i and 8a–h. E.S.-G. performed the experiment leading to Figs. 2d and 7c,d. L.M. constructed pBabe-RPS14-Myc, confirmed the qPCR in Supplementary Figs. 5c–,h,j–m and 6c–e. L.M. also performed cell culture experiments confirming Fig. 6a–h and Supplementary Fig. 8a–h. N.D.T performed ribosomes purification experiments. S.L.-P. participated in CX-5461 experiments. M.M. performed the FISH experiments leading to Fig. 1g–h and Supplementary Fig. 2. M.M. was the first to show nucleolar accumulation of RPL29. X.D.-S. did the bioinformatics analysis presented in Supplementary Fig. 3a. O.M. was the first to do the experiment on Supplementary Fig. 4f. M.-C.R. participated in qPCR optimization. C.E.Z. and D.Z. contributed by conceptual and technical input with FISH experiments. M.O. contributed by conceptual and technical input with northern blotting experiments. M.B. and B.L.C. performed the first experiment with CDK1/cyclin B1. B.L.C. also contributed by conceptual and technical input with IHC and helped with statistical analysis and IHC analysis. V.B. designed and performed many qPCR in Supplementary Fig. 1b–d and Supplementary Fig. 3b–d. F.L., V.B., D.Z., L.B.-G., M.O. and G.F. participated in experimental design. F.L. and G.F. wrote the manuscript.

Competing interests

The authors declare no competing interests.

Additional information

Supplementary information is available for this paper at https://doi.org/10.1038/s41556-018-0127-y.

Reprints and permissions information is available at www.nature.com/reprints.

Correspondence and requests for materials should be addressed to G.F.

Publisher's note: Springer Nature remains neutral with regard to jurisdictional claims in published maps and institutional affiliations.

Methods

Reagents. CX-5461 was purchased from Selleckchem (Cedarlane, Burlington, ON). Staurosporine, camptothecin and palbociclib (PD0332991) were purchased from Sigma-Aldrich (Oakville, ON). Interferon β-1a (ß-IFN) (Avonex, Biogen Idec) was a gift from D. P. Baker (Biogen Idec, Cambridge, MA).

Plasmids. Retroviruses pLPC, pLPC-3xFLAG, pBABE, pBABE-H-RasV12, pWZL, pWZL-H-RasV12 and pWZL-PML-IV were described previously[3]. pLXSN, pLXSN-E6, pLXSN-E7, pLXSN-E6/E7, pBABE-p16(WT), pBABE-CDK4(WT), pBABE-CDK6(WT) and pMLP-shp21 were a gift from S. W. Lowe (Memorial Sloan-Kettering Cancer Center, New York, NY). ShRb, shp16 and shNTC were subcloned in BglII/AgeI restriction sites to create retroviral vectors pMSCV-shRb, pMSCV-shp16, pMSCV-shNTC and pMLPX-shNTC (pMLPX is pMLP without GFP reporter). pLXSN-E7(Δ6-10), pLXSN-E7(Δ21-24) and pLXSN-E7(Δ79-83) were a gift from D. A. Galloway (Fred Hutchinson Cancer Center, Seattle, WA).

RSL1D1(WT) was PCR amplified and subcloned in BamHI/EcoRI restriction sites to create pBABE-RSL1D1(WT). pcDNA3.1-3xFLAG-RSL1D1 was made first by subcloning the PCR amplified 3xFLAG tag into EcoRV/EcoRI restriction sites of the vector pcDNA3.1(-) (Life Technologies, Invitrogen, Burlington, ON) to create pcDNA3.1-3xFLAG. Then RSL1D1(WT) was PCR amplified and subcloned in EcoRI/BamHI restriction sites to create pcDNA3.1-3xFLAG-RSL1D1(WT). CDK4(WT) and CDK4(K35M) were PCR amplified with primer containing the 3xFLAG tag and subcloned in BamHI/EcoRI restriction sites to create pBABE-3xFLAG-CDK4(WT) and pBABE-3xFLAG-CDK4(K35M). RPS14(WT)-Myc was PCR amplified from the vector pCMV6-RPS14-Myc-FLAG tagged (RC223055, Origene, Atlanta, GA) and subcloned in BamHI/SalI restriction sites to create pBABE-RPS14(WT)-Myc. RPS14(WT)-Myc was subcloned in BamHI/XhoI restriction sites to create retroviral vectors pMSCV-RPS14(WT)-Myc. RPS14(WT), RPS14(2-88) and RPS14(89-151) were PCR amplified and subcloned in BamHI/EcoRI restriction sites to create pcDNA3-FLAG-RPS14(WT), pcDNA3-FLAG-RPS14(2-88) and pcDNA3-FLAG-RPS14(89-151). Cyclin D1 was PCR amplified and subcloned in BamHI/EcoRI restriction sites to create pcDNA3-Myc-Cyclin D1(WT). For PCR primers used for cloning see Supplementary Table S4.

Lentiviruses pLKO expressing shRSL1D1 (shR-A, shR-B), shNS (shNS-A, shNS-B), shDDX21 (shD-A, shD-B), shEBP2 (shE-A, shE-B), shRPS14 (shRPS14-A, shRPS14-B) and shCTR were from Sigma-Aldrich (nos. 159162, 159486, 293679, 293681, 51198, 51199, 310234, 72461, 8643, 8644 and SHC002). Finally, pCMV-VSV-G (Addgene no. 8454) and pCMV-dR.91 (Delta8.9) were from R. Weinberg's laboratory (Whitehead Institute, Cambridge, MA). ShRNA target sequences are presented in Supplementary Table 3.

Cells and viral gene transfer. Phoenix ampho packaging cells were a gift from S. W Lowe. Human embryonic kidney HEK-293T cells, U2OS, PC3, H1299 were obtained from American Type Culture Collection (ATCC, Manassas, VA), normal human diploid fibroblasts IMR90 were obtained from the American Type Culture Collection or from Coriell Institute for Medical Research (Camden, NJ) and MUTZ-8 cells were obtained from the Leibniz Institute DSMZ-German Collection of Microorganisms and Cell Cultures (DSMZ no. ACC 689). PC3 cells were cultured in RPMI medium (Wisent, Montreal, QC) supplemented with 10% fetal bovine serum (FBS; Wisent), 1% penicillin/streptomycin (Wisent) and 2 mM L-glutamine (Wisent). MUTZ-8 cells were cultured in α-MEM (Invitrogen; cat. no. 12571063) supplemented with 20% fetal bovine serum (FBS; Wisent), 1% penicillin/streptomycin sulfate (Wisent) and 10 ng ml^{-1} of human recombinant GM-CSF (Peprotech; cat. no. 300-03-100ug). All other cell lines were cultured in Dulbecco's modified Eagle medium (DMEM; Wisent) supplemented with 10% FBS (Wisent) and 1% penicillin/streptomycin sulfate (Wisent).

Retroviral-mediated gene transfer was done as described[3]. For lentiviral transduction, 5×10^6 HEK-293 cells were seeded in 10 cm cell culture dishes and grown for 24 hours. Then, cells were transiently transfected using 2-3 µg of a lentiviral expression vector, 1 µg of the pCMV-VSV-G envelope protein expression plasmid and 2 µg of the pCMV-dR.91 (Delta8.9) plasmid containing *gag*, *pol* and *rev* genes in 900 µl of 1×Opti-MEM (Gibco Life Technologies, Burlington, ON). Then, 16 µl of X-tremeGENE 9 DNA Transfection reagent (Roche, Laval, QC) was added, tubes were inverted 4-5 times and after 10 min at room temperature, the mix was added to the cells. The medium was changed after 24 hours incubation. Supernatants from the transfected plates were collected 48 to 72 hours after transfection. The viral soups were filtered through a 0.45 µm filter, supplemented with 4 µg ml^{-1} polybrene (Sigma) and added on target cells. Twelve hours after the last infection, infected cell populations were selected using 2.5 µg ml^{-1} puromycin (Wisent) and/or 75 µg ml^{-1} hygromycin (Wisent) and/or 400 µg ml^{-1} G418 (Wisent).

Cell fractionation and immunoblotting. Cell fractions[41] and immunoblotting[23] were performed as previously described. For antibodies see Supplementary Table 6.

Cells proliferation and senescence analysis. Proliferation was assessed from estimations of cell number according to a crystal violet retention assay[3]. Senescence-associated-β-galactosidase (SA-β-gal) activity was assayed as described previously[3]. Source data for growth curves are presented in Supplementary Table 5.

Immunohistochemistry. Paraffin-embedded tissue samples were heated at 55 °C for 1 hour prior to deparaffinization and rehydration by sequential incubation in xylene (2×6 min), 100% ethanol (1×5 min), 95% ethanol (1×3 min), 75% ethanol (1×3 min) and 40% ethanol (1×3 min). Samples were washed in 1×TBS/0.3% Triton X-100 for 5 min and then in dH_2O for 3 min. Skin TMAs SK803 were bleached with the delicate melanin bleach kit for special stains and IHC (catalogue no. 24909-1, Polysciences, Warrington, PA). Antigen retrieval was performed by heating for 15 min at 95 °C in 10 mM citrate buffer (pH 6.0). Samples were cooled for at least 1 hour and washed 3 times for 3 min with 1×TBS/0.3% Triton X-100. Endogenous peroxidases were inactivated by incubation for 5 min at room temperature in a solution of 3% H_2O_2. Samples were washed 3 times for 3 min in 1×TBS/0.3% Triton X-100 and tissues were delimited using a hydrophobic barrier pen. Tissues were blocked 1 hour at room temperature with a protein-blocking serum-free ready-to-use reagent (DAKO, cat. no. X0909, Carpinteria, CA), and incubated overnight at 4 °C with primary antibodies diluted in 5% goat serum in 1×TBS/0.3% Triton X-100. Antibodies were: anti-INK4a (p16, p16INK4a) rabbit monoclonal (1:250, EPR1473, ab108349, lot: GR155011-2, Abcam, Toronto, ON) and anti-RPL29 rabbit polyclonal (1:250, GTX101833, lot: 40681, Gene Tex, Irvine, CA). Tissues were washed 3 times for 3 min in 1×TBS/0.3% Triton X-100 followed by primary antibody detection using the LSAB2 System-HRP (DAKO, cat. no. K0675, Carpinteria, CA), for 30 min using the secondary biotinylated antibody (DAKO, cat. no. K0675, Carpinteria, CA) then, tissues were washed 2 times for 5 min in 1×TBS/0.3% Triton X-100 and then incubated for 30 min with streptavidin-HRP (DAKO, cat. no. K0675, Carpinteria, CA). Tissues were washed 3 times for 3 min with 1×TBS/0.3% Triton X-100. Finally, the specimens were stained for peroxidase with Di-amine-benzidine (DAB) substrate kit (SK-4100, Vector Labs., Burlington, ON). The reaction was stopped by washing with water when the staining was sufficient; the same incubation time was applied to all samples. Tissues were counterstained with hematoxylin (HHS16, Sigma-Aldrich) and dehydrated by sequential incubation in 40% ethanol (1×1 min), 75% ethanol (1×1 min), 95% ethanol (1×1 min), 100% ethanol (1×1 min) and xylene (2×5 min). Finally, slides were mounted with Cytoseal 60 (8310-4, Thermo Scientific, Burlington, ON) and scanned with a NanoZoomer 2.0-HT scanner (Hamamatsu). Images were processed with NDP.view 2.6.8 (NanoZoomer Digital Pathology.view 2.6.8)(Hamamatsu).

We purchased TMAs from US Biomax (catalogue no. PR807a and SK803, Rockville, MD). SK803 is a skin basal cell carcinoma tissue microarray with 30 cases of skin basal cell carcinoma, 18 benign naevi and 3 normal skins (all in duplicate). PR807a is a prostatic adenocarcinoma, hyperplasia and normal tissue microarray with 50 prostate adenocarcinomas, 20 benign prostatic hyperplasia and 3 cases of normal prostate (single core per case). TMAs from US Biomax were reviewed by two board certified pathologists.

Immunofluorescence. Immunofluorescence images were performed as described[3]. For antibodies see Supplementary Table 6. Images were acquired with a FV300 Olympus confocal microscope with a PMT first generation and Fluoview V4.2 or a Zeiss Axio Imager Z2 upright microscope with a CoolSNAP FX camera (Photometrics) and/or Axiocam camera and ZEN 2 Imager (2.0.14283.302). Images were processed with ImageJ (2.0.0-rc-49/1.51 g).

For superresolution structured illumination microscopy, images were acquired with Super Resolution microscope Axio Observer Z1 ZEISS Elyra PS.1, from Zeiss. Raw data were captured using EMCCD Du885K ISO VP461 camera. Images were acquired at 5 rotations and final image was generated using the structured illumination algorithm of ZEN 2.1 (V11.0.0.190).

Fluorescence in situ hybridization (FISH). For FISH, 3×10^5 IMR90 cells were seeded onto 18 mm round glass coverslips overnight. Cells were washed once with 1×PBS at room temperature and fixed by 4% paraformaldehyde/1×PBS at room temperature for 10 min. Cells were washed twice with 1×PBS at room temperature for 5 min followed by a wash with 1.5 ml of 70% ethanol per well. To dehydrate, cells were sequentially incubated at room temperature in 70% ethanol (1×2 min), 85% ethanol (1×2 min), 100% ethanol (1×2 min), air dry at room temperature. To rehydrate, cells were incubated in 10% formamide/2×SSC at room temperature for 10 min. Cells were then washed in fresh prehybridization solution (10% formamide/2×SSC pH 7.2) for 10 min at room temperature. Antisense probe (5-ACTCCGGAGAGGGGTCGGAA-3) and sense probe (5-TTCCGACCCCTCTCCGGAGTC-3) were purchased already labelled with a fluorophore Alexa fluor 594 (Invitrogene). For each hybridization, 25 ng of the antisense probe was used or 50 ng of the sense probe. Probes were mixed with 20 µg of yeast tRNA:ssDNA, dried in a SpeedVac and dissolved in 40 µl of 1×hybridization solution (10% deionized formamide (Sigma)/10% dextran sulfate/2×SSC/2 mM VRC (RNAse inhibitor/1% BSA New England Biolabs, Whitby, ON) and heated for 3 min at 95 °C. Reconstituted probe were centrifuged for 3 min at 17,500×g, to eliminate any air from the sample. Probe hybridization mix was added to the cells, sealed with parafilm paper and incubated overnight in a humid chamber at 37 °C. Coverslips were transferred to a 12-well plate containing 10% formamide/2×SSC for 30 min at 37 °C protected from light. Then, cells were washed twice with 2×SSC for 30 min at room temperature. Cells were also washed with 1×PBS and mounted with ProLong Gold with DAPI (Molecular

Probe, Logan, UT). Images were acquired with a Zeiss Z2 upright microscope and processed with ImageJ. Statistics source data for FISH are presented in Supplementary Table 5.

Ribosome purification by sedimentation. To separate ribosomal RPS14 from non-ribosomal RPS14 we modified a previously used protocol to purify these fractions[42]. Cells were washed once with 10 ml of ice-cold 1× PBS on ice. After thoroughly removal of the 1× PBS, 400 µl of ice-cold lysis Polysome buffer: 20 mM Tris-HCl pH 7.4, 150 mM NaCl, 5 mM $MgCl_2$, 1 mM DTT, 1% Triton X-100 [BioShop], 25 U ml^{-1} of DNase I-RNAse free [Thermo Scientific] were added onto cells with a special attention to cover the entire surface of the dish. Cells were recovered by scrapping and clumps were dispersed by pipetting several times. Lysates were then transferred in a microfuge tube and incubated 10 min on ice. Then, lysates were centrifuged at 9,600 × g for 10 min at 4 °C to eliminate debris. To pellet ribosomes, 200 µl of supernatant were transferred to a 11 mm × 34 mm polycarbonate ultracentrifuge tube (Beckmam Coulter, no. 343778) and 600 µl of 1 M sucrose cushion (Polysome buffer, 1 M sucrose) were carefully added at the very bottom of the tube before centrifugation in a S150-AT rotor at 195,944 × g for 4 hours at 4 °C. Proteins from the supernatant were precipitated with methanol/chloroform. For 200 µl of supernatant, 800 µl of methanol were added and well vortexed. Then, 200 µl of chloroform were added and well vortexed. Then, 600 µl of ddH_2O was added and well vortexed. After a 5 min centrifugation at 17,000 × g, the top aqueous layer was discarded. Then, 800 µl of methanol were added, well vortexed, centrifuged 5 min at 17,000 × g. The latter protein pellets as well as the ribosomal pellets were resuspended in 2× Laemmli sample buffer (4% SDS, 20% glycerol, 120 mM Tris-HCl pH 6.8,) for immunoblotting analysis. Total RNA from 200 µl of supernatant was extracted with 800 µl of TRIzol (Invitrogen) while RNA from ribosomal pellets was extracted with 1 ml of TRIzol and resolved with a formaldehyde agarose gel.

RNA analysis, electrophoresis and northern blotting. Pulse labelling of rRNA synthesis was performed as previously described[41]. Northern blots were performed as previously described[43]. Briefly, total RNA extracts were prepared in TRIzol (Invitrogen) according to the manufacturer's instructions. Seven µg of total RNA from IMR90 cells were resolved on 1% agarose-formaldehyde gels in Tricine-Triethanolamine and transferred on nylon membrane in 10× SSC by capillarity. Probes were fluorescently labelled with DyLight 800 NHS Ester. The following probes were used: 5′ of ITS1 (position 5520) (^+H_4N-5′-cctcgccctccgggctccgttaatgatc-3′-NH_4^+), 3′ of ITS1 (position 6512) (^+H_4N-5′-cgcccaagaggagagggggttgcctcag-3′-NH_4^+) and ITS2 (position 7564) (^+H_4N-5′-gcgcgacggcggacgacaccgcggcgtc-3′-NH_4^+). Bands were acquired with an Infrared Imaging System (model: Odyssay, model no: 9120, LI-COR, Biosciences) and quantified using Adobe Photoshop. 18S and 28S rRNA levels were used as loading controls and detected with methylene blue staining. Statistics source data for northern blots are presented in Supplementary Table 5.

Immunoprecipitation. 5×10^6 or 1.5×10^6 HEK-293T cells were seeded in 10 or 6 cm cell culture dishes respectively and grown for 24 hours. Then, cells were transiently transfected using the calcium phosphate method with 15 µg (10 cm) or 5 µg (6 cm) of pcDNA3.1(C1)-3xFLAG or pcDNA3.1(C1)-3xFLAG-RSL1D1 and cells were scraped 24 hours later. Three 10 cm cell culture dishes for each condition were used for mass spectrometry and one 6 cm cell culture dish for each condition was used for confirmation experiments. IMR90 cells were co-infected with retroviruses containing pBABE-3xFLAG-CDK(K35M) or pLPC-3xFLAG and lentiviruses expressing shRSL1D1 (shR-A) and were scraped at day 10 post-infection. Forty 10 cm cell culture dishes for each condition were used for the mass spectrometry experiment. Co-immunoprecipitation and interaction domains mapping between CDK4 or Myc-cyclin D1 with FLAG-RPS14(WT) or FLAG-RPS14(2-88) or FLAG-RPS14(89-151) was confirmed in HEK-293 cells. Cells were transiently transfected using the calcium phosphate method with 15 µg (10 cm) of pcDNA3.1(C1)-3xFLAG, pcDNA3-FLAG-RPS14(WT), pcDNA3-FLAG-RPS14(2-88) or pcDNA3-RPS14(89-151) with pBABE-CDK4(WT) or pcDNA3-Myc-cyclin D1 in presence of 20 µM of MG132 (Sigma-Aldrich) for 12 hours and cells were scraped 24 hours post transfection. Co-immunoprecipitation between endogenous CDK4 and endogenous RPS14 was performed using two 10 cm cell culture dishes of PC3 cells or H1299 cells at 80% confluence for each condition.

Cells were scraped in IP buffer (50 mM Tris-HCl, pH 7.9, 1 mM EDTA, 0.1 mM EGTA, 12.5 mM $MgCl_2$, 400 mM NaCl, 20% glycerol, 1% Triton X-100 (BioShop), 0.1% SDS and 1× complete-EDTA free protease inhibitor cocktail (Roche Applied Science)). Cell lysates were kept on ice for 15 min and then sonicated for 40 seconds at the lowest intensity. Cell lysates were cleared by centrifugation at 16,300 × g for 1 min and immunoprecipitations were performed with anti-FLAG M2 Affinity Gel (no. A2220-5ML, lot: SLBT8835, Sigma-Aldrich, St Louis, MO) for 30 min at 4 °C. For endogenous interaction between CDK4 and RPS14, immunoprecipitations were performed with anti-RPS14 rabbit polyclonal (5 µg per condition, A304-031A, lot: A304-031A-1, Bethyl Laboratories) or rabbit pre-immune serum for 90 min at 4 °C. Then, immunoprecipitates were recovered with a 1:1 mix of protein-A and -G sepharose (Sigma-Aldrich). Protein-A/Protein-G sepharose mix and anti-FLAG M2 Affinity Gel were blocked for 1 hour at 4 °C in IP buffer containing 2.5% BSA, 0.16 µg $µl^{-1}$ salmon sperm DNA (Sigma-Aldrich) and 0.16 µg $µl^{-1}$ *E. coli* tRNA (Sigma-Aldrich) and then washed twice with IP buffer before immunoprecipitation. Immunoprecipitates were recovered after 30 min (45 min for endogenous IP) of incubation at 4 °C and washed three times for 30 min in IP buffer. Proteins of immunoprecipitates and total cell lysates were separated by SDS-PAGE and transferred to nitrocellulose membranes and analysed by Western Blotting with the antibodies described in the section Immunoblotting. For mass spectrometry analysis, proteins from immunoprecipitates were separated by SDS-PAGE, stained with Coomassie and gels from each condition were cut in four pieces for analysis by LC-MS/MS.

Liquid chromatography and mass spectrometry (LC-MS/MS). Bands were shrunk in 50% acetonitrile (ACN) and reconstituted in 50 mM ammonium bicarbonate with 10 mM TCEP and vortexed for 1 hour at 37 °C. Chloroacetamide was added for alkylation to a final concentration of 55 mM. Samples were vortexed for another hour at 37 °C prior to addition of 1 µg of trypsin and the digestion was left for 8 hours at 37 °C. Peptide extraction was conducted with 90% ACN. Extracted peptide samples were dried down and solubilized in 5% ACN/0.2% formic acid (FA). Samples were loaded on a homemade C18 precolumn (0.3 mm i.d. x 5 mm) connected directly to the switching valve and separated on a homemade reversed-phase column (150 µm i.d. x 150 mm) with a 56-min gradient from 10–30% acetonitrile (0.2% FA) and a 600 nl min^{-1} flow rate on a NanoLC-2D system (Eksigent, Dublin, CA) connected to an Q-Exactive Plus (Thermo Fisher Scientific). Each full MS spectrum acquired with a 60,000 resolution was followed by 12 MS/MS spectra, where the 12 most abundant multiply charged ions were selected for MS/MS sequencing. Tandem MS experiments were performed using HCD. The data were processed using PEAKS 7.0 (Bio-informatics Solutions, Waterloo, ON) and the Uniprot database. Tolerances on precursors and fragments were 15 ppm and 0.01 Da, respectively. Variable selected post-translational modifications were carbamidomethyl (C), oxidation (M), deamidation (NQ) and phosphorylation (STY).

Bioinformatic analysis of data from LC-MS/MS. After the protein identification described above, the full list of all proteins was analysed using the FatiGO analysis tool[44] on the Babelomics 4.3 and 5.0 platforms. In order to identify overrepresented groups, the identified proteins were compared to the whole genome protein list provided by the Babelomics platform (http://babelomics.bioinfo.cipf.es/). The databases used were GO biological process, GO molecular function and GO cellular component. Significance was determined using a two-tailed Fisher exact test. The GO terms and their associated proteins were then grouped in general categories based on knowledge and literature.

In vitro protein phosphorylation. Recombinant RPS14-Myc-FLAG was produced in HEK-293 cells transiently transfected using the calcium phosphate method with 15 µg (10 cm) of pCMV6-RPS14-Myc-FLAG and then immunoprecipitated with anti-FLAG M2 Affinity Gel as previously described, washed three times for 5 min in 1× TBS, eluted for 1 hour at 4 °C with 250 ng $µl^{-1}$ of FLAG peptide (Sigma-Aldrich) in 1× TBS and protein concentration was evaluated using a NanoDrop2000c spectrophotometer (A280).

Human active CDK4/cyclin D1 (cat. no. C0620, lot SLBK7657V, Sigma-Aldrich, St. Louis, MO) or human active CDK1/cyclin B1 (cat. no. C22-10G, lot: E094-1, SignalChem, Richmond, BC) were incubated alone or with human recombinant GST-Rb (773-928) (cat. no. R05-55G, lot M166-3, SignalChem) in presence or absence of palbociclib (1 µM) or staurosporine (1 µM) or with a gradient of human recombinant RPS14-Myc-FLAG in kinase assay buffer I (cat. no. K01-09, SignalChem): 25 mM MOPS, pH 7.2, 12.5 mM ß-glycerol-phosphate, 25 mM $MgCl_2$, 5 mM EGTA, 2 mM EDTA, 0.25 mM dithiothreitol (DTT), 40 µM ATP with or not 1 µCi (γ-^{32}P)ATP at 30 °C for 30 min. Then Laemmli buffer was added to stop the reaction, samples were boiled at 98 °C for 5 min and the reaction products were separated by SDS-PAGE, transferred to nitrocellulose membranes and ^{32}P incorporation was analysed by autoradiography and quantified with Adobe Photoshop. Total proteins were visualized with Ponceau. IC_{50} of RPS14 on 0.5 µg of CDK4/cyclin D1 was determined by quantifying ^{32}P incorporation in function of RPS14 amount from three independent experiments.

In vitro protein interaction (GST pulldown assay). Human recombinant RPS14-Myc-FLAG was produced as previously described (see 'In vitro protein phosphorylation'). GST (50 ng) (cat. no. SRP5348, lot: F664-2, Sigma-Aldrich, St Louis, MO) or GST tagged human active CDK4/cyclin D1 (50 ng) (cat. no. C0620, lot: SLBK7657V, Sigma-Aldrich) or GST tagged human CDK4 (50 ng) (cat. no. C31-14G, lot: K127-1, Signal Chem, Richmond, BC) or GST tagged human cyclin D1 (50 ng) (cat. no. 009-001-153 S, lot: 37136, Rockland Antibodies & Assays, Limerick, PA) were incubated with human recombinant RPS14-Myc-FLAG (200 ng) in 300 µl of PB buffer (20 mM Hepes, pH 7.5, 130 mM KCl, 5 mM $MgCl_2$, 1 mM DTT, 0.5 mM EDTA, 0.05% NP40) and mixed using a rotating machine at 30 °C for 2 hours. Proper amounts of glutathione-Sepharose beads (cat. no. 17-0756-01, GE Healthcare, Sweden) were washed three times with PB buffer. Then, 10 µl of glutathione beads and 5 µl of BSA (25% stock solution) were added to proteins mix and incubation continued at room temperature for

30 min with rotation. The beads were then washed three times for 15 minutes with PB buffer at room temperature with rotation. Then, the appropriated quantity of 6× loading buffer (0.5 M Tris-HCl pH6.8, 30% glycerol, 10% SDS, 1% bromophenol blue and 15% β-mercaptoethanol) was added. The samples were boiled for 5 min and separated by SDS-PAGE for western blotting.

Real-time PCR. Total RNA extracts were prepared in TRIzol (Invitrogen) according to the manufacturer's instructions. Total RNA was reverse transcribed and gene expression level was determined with a LightCycler 480 (software release 1.5.1.62 SP2) and/or a LightCycler 96 (software version 1.1) Real-Time PCR System (Roche Applied Science), using SYBR Green technologies as described before[3]. qPCR primers are presented in Supplementary Table 4. Source data for qPCR are presented in Supplementary Table 5.

Statistics and reproducibility. Statistical analysis (two-tailed Student's *t*-test) was performed using Excel and (Mann–Whitney U test) was performed using Statistica software (StatSoft, Tulsa, OK). A value of $P < 0.05$ was considered statistically significant. Experiments were repeated at least three times, except for those in Figs. 1g–h, 2d, 5c and 6j–m and Supplementary Figs. 2a–c, 3e–g,i–j, 4a,f, 5b (CDK6), 5c–m, 6a–e,i, 7a (PML), 7b–c and 8a–h, which were repeated twice, and Supplementary Figs. 3b–d, 4b–e,g–j, 5a (CDK6) and Supplementary Tables 1 and 2, which were performed once. Experiments that were only performed once or twice include three technical replicates except Fig. 5c where immunoblots were preformed using two independent shRNAs and Fig. 6k where immunoblots were performed twice. Also in many instances of 1 or 2 independent experiments data were collected from replicates of two independent shRNAs or in different models of senescence adding robustness to the results. For SA-β-Gal, data were quantified from many fields within one experiment to properly represent the entire petri dish and subsequently confirmed as described in figure captions. For IF, data were quantified from three technical counts within one experiment and subsequently confirmed as described in figure captions.

Reporting Summary. Further information on experimental design is available in the Nature Research Reporting Summary linked to this article.

Data availability. Mass spectrometry data have been deposited in ProteomeXchange with the primary accession code PASS01176. Source data for Figs. 1e–f, 4h, 5a–b, 6a,c,e,g,i,l–m and 7d and Supplementary Figs. 1b–d, 2d–e, 3b–g,i–j, 4b–j, 5b–h,j–m, 6a–e,i and 8a,c,e,g can be found in Supplementary Table 5. All other data that support the findings of this study are available from the corresponding author upon reasonable request.

References

41. Lessard, F. et al. The ARF tumor suppressor controls ribosome biogenesis by regulating the RNA polymerase I transcription factor TTF-I. *Mol. Cell* **38**, 539–550 (2010).
42. Ingolia, N. T., Brar, G. A., Rouskin, S., McGeachy, A. M. & Weissman, J. S. The ribosome profiling strategy for monitoring translation in vivo by deep sequencing of ribosome-protected mRNA fragments. *Nat. Protoc.* **7**, 1534–1550 (2012).
43. Scott, D. D. et al. Nol12 is a multifunctional RNA binding protein at the nexus of RNA and DNA metabolism. *Nucleic Acids Res.* **45**, 12509–12528 (2017).
44. Al-Shahrour, F., Diaz-Uriarte, R. & Dopazo, J. FatiGO: a web tool for finding significant associations of Gene Ontology terms with groups of genes. *Bioinformatics* **20**, 578–580 (2004).

nature research

Corresponding author(s): Gerardo Ferbeyre

Reporting Summary

Nature Research wishes to improve the reproducibility of the work that we publish. This form provides structure for consistency and transparency in reporting. For further information on Nature Research policies, see Authors & Referees and the Editorial Policy Checklist.

Statistical parameters

When statistical analyses are reported, confirm that the following items are present in the relevant location (e.g. figure legend, table legend, main text, or Methods section).

n/a	Confirmed	
☐	☒	The exact sample size (*n*) for each experimental group/condition, given as a discrete number and unit of measurement
☐	☒	An indication of whether measurements were taken from distinct samples or whether the same sample was measured repeatedly
☐	☒	The statistical test(s) used AND whether they are one- or two-sided *Only common tests should be described solely by name; describe more complex techniques in the Methods section.*
☒	☐	A description of all covariates tested
☒	☐	A description of any assumptions or corrections, such as tests of normality and adjustment for multiple comparisons
☐	☒	A full description of the statistics including central tendency (e.g. means) or other basic estimates (e.g. regression coefficient) AND variation (e.g. standard deviation) or associated estimates of uncertainty (e.g. confidence intervals)
☐	☒	For null hypothesis testing, the test statistic (e.g. *F*, *t*, *r*) with confidence intervals, effect sizes, degrees of freedom and *P* value noted *Give P values as exact values whenever suitable.*
☒	☐	For Bayesian analysis, information on the choice of priors and Markov chain Monte Carlo settings
☒	☐	For hierarchical and complex designs, identification of the appropriate level for tests and full reporting of outcomes
☒	☐	Estimates of effect sizes (e.g. Cohen's *d*, Pearson's *r*), indicating how they were calculated
☐	☒	Clearly defined error bars *State explicitly what error bars represent (e.g. SD, SE, CI)*

Our web collection on statistics for biologists may be useful.

Software and code

Policy information about availability of computer code

Data collection	Immunofluorescence and Fluorescence In Situ Hybridization : Image acquisition with ZEN 2 Imager (2.0.14283.302) (Zeiss). Superresolution microscopy : Final image was generated using the structured illumination algorithm of ZEN 2.1 (V11.0.0.190) (Zeiss). Real-time PCR: Data collection with a LightCycler 480 (software release 1.5.1.62 SP2) and/or a LightCycler 96 (software version 1.1).
Data analysis	Immunohistochemistry: Images were processed with NDP.view 2.6.8 (Hamamatsu Photonics). Immunofluorescence and Fluorescence In Situ Hybridization: Images were processed with Image J (2.0.0-rc-49/1.51g). Liquid Chromatography and mass spectrometry (LC-MS/MS): The data were processed using PEAKS 7.0 (Bio-informatics Solutions). Bioinformatic of LC-MS/MS : With FatiGO analysis tool on the Babelomics 4.3 and 5.0 platforms (http://babelomics.bioinfo.cipf.es/). Real-time PCR: With a LightCycler 480 (software release 1.5.1.62 SP2) and/or a LightCycler 96 (software version 1.1).

For manuscripts utilizing custom algorithms or software that are central to the research but not yet described in published literature, software must be made available to editors/reviewers upon request. We strongly encourage code deposition in a community repository (e.g. GitHub). See the Nature Research guidelines for submitting code & software for further information.

Data

Policy information about availability of data

All manuscripts must include a data availability statement. This statement should provide the following information, where applicable:

- Accession codes, unique identifiers, or web links for publicly available datasets
- A list of figures that have associated raw data
- A description of any restrictions on data availability

The datasets that support the findings of this study are available upon reasonable request from the first and the corresponding author.

Field-specific reporting

Please select the best fit for your research. If you are not sure, read the appropriate sections before making your selection.

☒ Life sciences ☐ Behavioural & social sciences

For a reference copy of the document with all sections, see nature.com/authors/policies/ReportingSummary-flat.pdf

Life sciences

Study design

All studies must disclose on these points even when the disclosure is negative.

Sample size	No sample size calculations were performed. Sample size was determined after discussions with team members and from our experience on calculating statistical signicance. For SA-beta-gal, data were quantified from many fields to properly represent the entire petri dish. For IF, data were quantified from 100 cell counts in triplicate to properly represent the entire petri dish. For QPRC, data were derived from technical triplicates. For northern blots, data were derived from biological triplicates. For growth-curves, data were derived from 3 different petri dishs. For nucleolar area and mean intensity, data were quantified from more than 90 nucleolus to properly represent variability between cells and conditions. For superresolution microscopy, the number of cells taken is related to time and space for data. For more precision, see figure legends and methods.
Data exclusions	We did not take in consideration the 7 samples of cancer adjacent normal prostate tissue from the prostate tissue microarray. Our objective was to compare normal tissue, cancer tissue and benign prostatic hyperplasia. Those excluded samples have a genetic backgroud leading to tumorigenesis and we wanted to take in consideration only real normal tissue.
Replication	All n are identified in figure legends. Experiments are reproducible and unreproducible experiments are not presented in this paper. Mass spectrometry experiments have been done once but interaction important for this article were replicated.
Randomization	Allocation was not random. Covariates were controlled: By using control empty vectors, control shRNA and independent shRNA. By doing time courses. By comparing different models of senescence. By studying senescence phenotypes with different markers and with different technics. By using different cell lines. By showing protein interactions with different technics as mass spectrometry, overexpression, mapping, at the endogenous level, in vitro interaction and with kinase assay.
Blinding	Blinding was not relevant to our study considering that for all cellular experiments different extracts were analysed by different persons. See authors' contributions for a description of how people reproduced data from other people.

Materials & experimental systems

Policy information about availability of materials

n/a	Involved in the study
☐	☒ Unique materials
☐	☒ Antibodies
☐	☒ Eukaryotic cell lines
☒	☐ Research animals
☒	☐ Human research participants

Unique materials

Obtaining unique materials	anti-UBF(#8) rabbit polyclonal (1 :1000, clone #8) was raised against mouse UBF (aa 2-404) and kindly provided by Dr. Tom Moss (Centre de recherche sur le cancer, Université Laval, QC). -The amount of the antibody is limited, but Dr. Tom Moss regularly provide aliquots. Interferon beta-1a (ß-IFN) (Avonex, Biogen Idec) was a gift from Dr. Darren P. Baker (Biogen Idec, Cambridge, MA). -This protein is commercially available.

Antibodies

Antibodies used

Antibodies identification (see Supplementary Table 6).

For IHC:
anti-INK4a rabbit monoclonal (1:250, EPR1473, lot : GR155011-2 , ab108349, Abcam, Toronto, ON).
anti-RPL29 rabbit polyclonal (1:250, GTX101833, lot : 40681, Gene Tex, Irvine, CA).

For IF:
anti-FBL rabbit monoclonal (1:350, clone C13C3, #2639, lot : 2, Cell Signaling Technology, Pickering, ON).
anti-RPL29 mouse polyclonal (1:125, #H00006159-B01P, lot : 10230, Novus Biologicals, Oakville, ON).
anti-RPS14 rabbit polyclonal (1:80, clone H-130, sc-68873, lot : C1914, Santa Cruz Biotechnology, Santa Cruz, CA).
anti-53BP1 rabbit polyclonal (1:200, Ab-1, Cat# PC712, lot : D00137736, Calbiochem, EMD Biosciences, San Diego, CA).
anti-phospho-gammaH2A.XS139 mouse monoclonal (1:100, JBW-301, Cat# 05-636-I, lot : 2552645, Millipore, Billerica, MA).
anti-cyclin D1 mouse monoclonal (1:60, clone HD11, sc-246, lot : D2108 , Santa Cruz Biotechnology, Santa Cruz, CA).
anti-PML rabbit polyclonal (1:200, A301-167A, lot : A301-167A-2, Bethyl Laboratories).
goat anti-rabbit IgG (H+L) conjugated to Alexa Fluor 488 (1:1000, #A11008, lot: 1166843, Molecular Probes, Invitrogen, Eugene, OR).
goat anti-mouse IgG (H+L) conjugated to Alexa Fluor 488 (1:1000, #A11029, lot: 1423008, Life Technologies, Eugene, OR).
goat anti-rabbit IgG (H+L) conjugated to Alexa Fluor 568 (1:1000, #A11036, lot: 1504529, Life Technologies, Eugene, OR).
goat anti-mouse IgG (H+L) conjugated to Alexa Fluor 568 (1:1000, #A11031, lot: 1398018, Life Technologies, Eugene, OR).

For IP:
anti-RPS14 rabbit polyclonal (5 µg per condition, A304-031A, lot : A304-031A-1, Bethyl Laboratories, Montgomery TX).
anti-FLAG mouse monoclonal Affinity Gel (#A2220-5ML, lot: SLBT8835, Sigma-Aldrich, St. Louis, MO).

For WB:
anti-H-RAS mouse monoclonal (1:250, clone F235, Sc-29, lot : C0608, Santa Cruz Biotechnology, Santa Cruz, CA).
anti-PML rabbit polyclonal (1:1000, A301-167A, lot : A301-167A-2, Bethyl Laboratories, Montgomery, TX).
anti-phospho-H3S10 rabbit polyclonal (1:1000, #06-570, lot : 2517793, Millipore, Billerica, MA).
anti-RSL1D1 goat polyclonal (1:1000, GTX88161, lot : 821500642, GeneTex, San Antonio, TX).
anti-RSL1D1 rabbit polyclonal (1:4000, HPA043483, lot : R40297, Sigma-Aldrich).
anti-NS rabbit polyclonal (1:1000, clone H-270, Sc-67012, lot : G1009, Santa Cruz Biotechnology, Santa Cruz, CA).
anti-DDX21 rabbit polyclonal (1:1000, GTX115199, lot : 40618, GeneTex).
anti-EBP2 goat polyclonal (1:500, clone N-13, sc-46316, lot : H1611, Santa Cruz Biotechnology, Santa Cruz, CA).
anti-MCM6 rabbit polyclonal (1:1000, A300-194A, lot : A300-194A-2, Bethyl Laboratories).
anti-p53 mouse monoclonal (1:1000, clone DO-1, Sc-126, lot : C1413, Santa Cruz Biotechnology, Santa Cruz, CA).
anti-phospho-p53S15 rabbit polyclonal (1:500, #9284, lot : 9, Cell Signaling).
anti-FLAG mouse monoclonal (1:1000, F1804, M2, lot : SLBK1346V, Sigma-Aldrich).
anti-c-Myc rabbit polyclonal (1:1000, clone A-14, sc-789, lot : K0215, Santa Cruz Biotechnology, Santa Cruz, CA).
anti-Myc tag mouse monoclonal (1:2000, 9E10, lot : 114K4821, Sigma, Saint Louis, Missouri).
anti-phospho-RBS795 rabbit polyclonal (1:500, #9301, lot : 13, Cell Signaling).
anti-RB mouse monoclonal (1:1000, clone G3-245, #554136, lot : 71957, BD Pharmingen).
anti-RPL29 rabbit polyclonal (1:1000, GTX101833, lot : 40681, GeneTex, Irvine, CA).
anti-RPS14 rabbit polyclonal (1:1000, clone H-130, sc-68873, lot : C1914, Santa Cruz Biotechnology, Santa Cruz, CA).
anti-RPS14 rabbit polyclonal (1:4000, A304-031A, lot : A304-031A-1, Bethyl Laboratories, Montgomery TX).
anti-RPS3 mouse monoclonal (1:1000, clone C-7, sc-376008, lot : D2116, Santa Cruz Biotechnology, Santa Cruz, CA).
anti-CDK4 rabbit polyclonal (1:2000, A304-225A, lot : A304-225A-1, Bethyl Laboratories).
anti-α-Tubulin mouse monoclonal (1:20000, clone B-5-1-2, T6074, lot : 023M4813, Sigma-Aldrich).
anti-GST mouse monoclonal (1:2000, clone GST-2, G1160, lot : 012M4814, Sigma-Aldrich).
anti-H3 rabbit polyclonal (1:2000, clone ab1791, lot : GR206453-1, Abcam).
anti-CDK4(HRP) rabbit monoclonal (1:2000, clone ab193968, lot : GR205710-1, Abcam).
anti-UBF(#8) rabbit polyclonal (1 :1000, clone #8) was raised against mouse UBF (aa 2-404) and kindly provided by Dr. Tom Moss (Centre de recherche sur le cancer, Université Laval, QC).
goat anti-rabbit IgG (H-L) conjugated to HRP (1:3000, #170-6515, lot: 64126042, Bio-Rad, Mississauga, ON).
goat anti-mouse IgG (H-L) conjugated to HRP (1:3000, #170-6516, lot: 64132955, Bio-Rad, Mississauga, ON).
donkey anti-goat IgG conjugated to HRP (1:3000, Sc-2020, lot: E2313, Santa Cruz Biotechnology, Santa Cruz, CA).

Validation

Antibodies identification (see Supplementary Table 6).

For IHC:
anti-INK4a rabbit monoclonal (1:250, EPR1473, lot : GR155011-2 , ab108349, Abcam, Toronto, ON). Tested by western blot (WB) after overexpression of human INK4a and by IHC on human samples. Cited 24 times on company website (Many for WB and IHC in human).

anti-RPL29 rabbit polyclonal (1:250, GTX101833, lot : 40681, Gene Tex, Irvine, CA). Tested by western blot on IMR90 cells and by IHC on human samples. Tested by company for IHC and WB on human cell lines.

For IF:
anti-FBL rabbit monoclonal (1:350, clone C13C3, #2639, lot : 2, Cell Signaling Technology, Pickering, ON). Tested by WB on IMR90 cells. Cited 17 times on company website. Tested by company for IF and WB on human cells.

anti-RPL29 mouse polyclonal (1:125, #H00006159-B01P, lot : 10230, Novus Biologicals, Oakville, ON). We used and tested this antibody only for IF. Tested by company for IHC, IF and WB of human cells.

anti-RPS14 rabbit polyclonal (1:80, clone H-130, sc-68873, lot : C1914, Santa Cruz Biotechnology, Santa Cruz, CA). Tested by WB after depletion of RPS14 with two different shRNA in many human cell lines and by IF on IMR90 cells. Cited 3 times on company website. Tested by company or reviewer for WB, IF and IHC on human cells.

anti-53BP1 rabbit polyclonal (1:200, Ab-1, Cat# PC712, lot : D00137736, Calbiochem, EMD Biosciences, San Diego, CA). We routinely use this antibody for IF. On company website : Key applications are IF, WB and IP. Works for human and mouse.

anti-phospho-gammaH2A.XS139 mouse monoclonal (1:100, JBW-301, Cat# 05-636-I, lot : 2552645, Millipore, Billerica, MA). We routinely use this antibody for IF. On company website : Well published antibody validated in ChIP, ICC, IF and WB. Works for human, mouse and rat.

anti-cyclin D1 mouse monoclonal (1:60, clone HD11, sc-246, lot : D2108 , Santa Cruz Biotechnology). Cited 189 times on company website. We used and tested this antibody only for IF. Tested by company or reviewer for WB, IF and IHC on human cells.

anti-PML rabbit polyclonal (1:200, A301-167A, lot : A301-167A-2, Bethyl Laboratories). Cited 37 times on company website. We used and tested this antibody for WB and IF on human IMR90 cells. Tested by company for WB, IP, IHC and IF on human cells.

goat anti-rabbit IgG (H+L) conjugated to Alexa Fluor 488 (1:1000, #A11008, lot: 1166843, Molecular Probes, Invitrogen, Eugene, OR). We routinely use this antibody for IF. On company website : More than 50 000 published references, applications and experimental tips.

goat anti-mouse IgG (H+L) conjugated to Alexa Fluor 488 (1:1000, #A11029, lot: 1423008, Life Technologies, Eugene, OR). We routinely use this antibody for IF. On company website : More than 50 000 published references, applications and experimental tips.

goat anti-rabbit IgG (H+L) conjugated to Alexa Fluor 568 (1:1000, #A11036, lot: 1504529, Life Technologies, Eugene, OR). We routinely use this antibody for IF. On company website : More than 50 000 published references, applications and experimental tips.

goat anti-mouse IgG (H+L) conjugated to Alexa Fluor 568 (1:1000, #A11031, lot: 1398018, Life Technologies, Eugene, OR). We routinely use this antibody for IF. On company website : More than 50 000 published references, applications and experimental tips.

For IP:
anti-RPS14 rabbit polyclonal (5 µg per condition, A304-031A, lot : A304-031A-1, Bethyl Laboratories, Montgomery TX). Tested by IP (PC3 and NCI-H1299) and WB on many human cell lines. Tested by company for IP and WB on human cells.

anti-FLAG mouse monoclonal Affinity Gel (#A2220-5ML, lot: SLBT8835, Sigma-Aldrich, St. Louis, MO). Cited 300 times on company website. Tested for IP after overexpression of different Flag-tagged-proteins.

For WB:
anti-H-RAS mouse monoclonal (1:250, clone F235, Sc-29, lot : C0608, Santa Cruz Biotechnology, Santa Cruz, CA). Cited 64 times on company website. Tested by WB after overexpression of H-RASv12 in IMR90 cells. Tested by company or reviewer for WB and IHC on human cells.

anti-PML rabbit polyclonal (1:1000, A301-167A, lot : A301-167A-2, Bethyl Laboratories, Montgomery, TX). Cited 37 times on company website. We used and tested this antibody for WB and IF on human IMR90 cells. Tested by company for WB, IP, IHC, IF and PLA (proximity ligation assay) on human cells.

anti-phospho-H3S10 rabbit polyclonal (1:1000, #06-570, lot : 2517793, Millipore, Billerica, MA). Tested by WB after different induction of cell cycle arrest. On company website : This highly published antibody has been validated in ICC, IP and WB. Works for human and mouse.

anti-RSL1D1 goat polyclonal (1:1000, GTX88161, lot : 821500642, GeneTex, San Antonio, TX). Tested by WB after depletion of RSL1D1 with two different shRNA in human IMR90 cells. Tested by company for WB on human cells.

anti-RSL1D1 rabbit polyclonal (1:4000, HPA043483, lot : R40297, Sigma-Aldrich). Tested by WB and IHC on human cells. On company website : (Human Protein Atlas) This antibody has been used for staining of 44 normal human tissue samples as well as human cancer samples covering the 20 most common cancer types and up to 12 patients for each cancer type.

anti-NS rabbit polyclonal (1:1000, clone H-270, Sc-67012, lot : G1009, Santa Cruz Biotechnology). Tested by WB after depletion of NS with two different shRNA in human IMR90 cells. Tested by company for WB and IF on human cells.

anti-DDX21 rabbit polyclonal (1:1000, GTX115199, lot : 40618, GeneTex). Tested by WB after depletion of DDX21 with two different shRNA in human IMR90 cells. Tested by company for WB and IF on human cells.

anti-EBP2 goat polyclonal (1:500, clone N-13, sc-46316, lot : H1611, Santa Cruz Biotechnology). Tested by WB after depletion of EBP2 with two different shRNA in human IMR90 cells. Tested by company for WB and IF on human cells.

anti-MCM6 rabbit polyclonal (1:1000, A300-194A, lot : A300-194A-2, Bethyl Laboratories). Cited 6 times on company website. We routinely use this antibody for WB and tested by WB after different induction of cell cycle arrest. Tested by company for WB

and IHC on human cells.

anti-p53 mouse monoclonal (1:1000, clone DO-1, Sc-126, lot : C1413, Santa Cruz Biotechnology). Cited 1668 times on company website. Tested by WB and IF. Tested by company for WB, IF and IHC.

anti-phospho-p53S15 rabbit polyclonal (1:500, #9284, lot : 9, Cell Signaling). Cited 506 times on company website. Used for WB after nucleolar stress or induction of senescence.

anti-FLAG mouse monoclonal (1:1000, F1804, M2, lot : SLBK1346V, Sigma-Aldrich). Cited 387 times on company website. Tested for WB and IP after overexpression of different Flag-tagged-proteins.

anti-c-Myc rabbit polyclonal (1:1000, clone A-14, sc-789, lot : K0215, Santa Cruz Biotechnology). Cited 429 times on company website. Tested for WB after overexpression of Myc-tagged-proteins. Tested by company for WB and IF after overexpression of Myc-tagged-proteins.

anti-Myc tag mouse monoclonal (1:2000, 9E10, lot : 114K4821, Sigma, Saint Louis, Missouri). Cited 1036 times on company website. Tested for WB after overexpression of Myc-tagged-proteins. Tested by company for WB and IF after overexpression of Myc-tagged-proteins.

anti-phospho-RBS795 rabbit polyclonal (1:500, #9301, lot : 13, Cell Signaling). Cited 74 times on company website. We routinely use this antibody for WB and tested by WB after different induction of cell cycle arrest. Tested by company for WB on human cells.

anti-RB mouse monoclonal (1:1000, clone G3-245, #554136, lot : 71957, BD Pharmingen). 9 references on company website. Tested by WB on human cells. Tested by company for WB and IF on human cell lines.

anti-RPL29 rabbit polyclonal (1:1000, GTX101833, lot : 40681, GeneTex, Irvine, CA). Tested by western blot on IMR90 cells and by IHC on human samples. Tested by company for IHC and WB on human cell lines.

anti-RPS14 rabbit polyclonal (1:1000, clone H-130, sc-68873, lot : C1914, Santa Cruz Biotechnology, Santa Cruz, CA). Tested by WB after depletion of RPS14 with two different shRNA in many human cell lines and by IF on IMR90 cells. Cited 3 times on company website. Tested by company or reviewer for WB, IF and IHC on human cells.

anti-RPS14 rabbit polyclonal (1:4000, A304-031A, lot : A304-031A-1, Bethyl Laboratories, Montgomery TX). Tested by IP and WB on human cell lines. Tested by company for IP and WB on human cells.

anti-RPS3 mouse monoclonal (1:1000, clone C-7, sc-376008, lot : D2116, Santa Cruz Biotechnology). Tested for WB on different human cell lines. Tested by company or reviewer for WB and IHC on human cells.

anti-CDK4 rabbit polyclonal (1:2000, A304-225A, lot : A304-225A-1, Bethyl Laboratories). Tested for WB and IP on human cells. Tested by company for WB, IP and IHC on human cells.

anti-α-Tubulin mouse monoclonal (1:20000, clone B-5-1-2, T6074, lot : 023M4813, Sigma-Aldrich). Cited 449 times on company website. Tested for WB on human cells. Tested by company for WB, and IF on human cells.

anti-GST mouse monoclonal (1:2000, clone GST-2, G1160, lot : 012M4814, Sigma-Aldrich). Cited 57 times on company website. Tested on many purchased GST-tagged recombinant proteins. Tested by company on GST purified protein by WB.

anti-H3 rabbit polyclonal (1:2000, clone ab1791, lot : GR206453-1, Abcam). Cited 1477 times on company website. Tested for WB on IMR90 cells. Tested by company for WB, IP, IF, IHC and ChIP on human cell lines.

anti-CDK4(HRP) rabbit monoclonal (1:2000, clone ab193968, lot : GR205710-1, Abcam). Tested for WB on PC3 and NCI-H1299 human cell lines. Tested by company for WB and IHC on human cells.

anti-UBF(#8) rabbit polyclonal (1 :1000, clone #8) was raised against mouse UBF (aa 2-404) and kindly provided by Dr. Tom Moss (Centre de recherche sur le cancer, Université Laval, QC). Tested by WB and IF on IMR90 cells. This antibody is also working by WB and IF on mouse cells.
See :
1-Hamdane, N. et al. (2014). Conditional Inactivation of Upstream Binding Factor Reveals Its Epigenetic Functions and the Existence of a Somatic Nucleolar Precursor Body. PLoS Genet 10(8): e1004505. https://doi.org/10.1371/journal.pgen.1004505
2-Lessard, F. et al. (2010). The ARF tumor suppressor controls ribosome biogenesis by regulating the RNA polymerase I transcription factor TTF-I. Mol Cell 38, 539-550.

goat anti-rabbit IgG (H-L) conjugated to HRP (1:3000, #170-6515, lot: 64126042, Bio-Rad, Mississauga, ON). We routinely use this antibody for WB. Cited 125 times on company website.

goat anti-mouse IgG (H-L) conjugated to HRP (1:3000, #170-6516, lot: 64132955, Bio-Rad, Mississauga, ON). We routinely use this antibody for WB. Cited 104 times on company website.

donkey anti-goat IgG conjugated to HRP (1:3000, Sc-2020, lot: E2313, Santa Cruz Biotechnology). We routinely use this antibody for WB. Cited 677 times on company website.

Eukaryotic cell lines

Policy information about cell lines

Cell line source(s)	Phoenix ampho packaging cells were a gift from S. W Lowe. (HEK)-293T, U2OS, PC3 and H1299 cells were obtained from American Type Culture Collection (ATCC, Manassas, VA). IMR90 cells were obtained from the American Type Culture Collection (ATCC, Manassas, VA) and/or from Coriell Institute for Medical Research (Camden, NJ). MUTZ-8 cells were obtained from the Leibniz Institute DSMZ-German Collection of Microorganisms and Cell Cultures
Authentication	Certificate of authentification was provided for normal human fibroblasts IMR90 cells from Coriell. MUTZ-8 cells underwent a careful identity control in the Leibniz Institute : https://www.dsmz.de/catalogues/catalogue-human-and-animal-cell-lines/quality-assurance/identity-control.html. All other cell lines comes from ATCC and we confirmed their key molecular characteristics relevant for our study: H1299 and PC3 are p53 negative, U2OS are p53 wild type. Also their morphology is the same as published in many other papers with these cell lines. Phoenix ampho packaging cells were not authentified and were used only for retrovirus production.
Mycoplasma contamination	All cell lines tested negative for mycoplasma contamination.
Commonly misidentified lines (See ICLAC register)	(HEK) 293T cells : We use them for retroviral and lentiviral production, coimmunoprecipitation after overexpression of recombinant proteins and purification of recombinant proteins.

Method-specific reporting

n/a	Involved in the study
☒	☐ ChIP-seq
☒	☐ Flow cytometry
☒	☐ Magnetic resonance imaging